

Aerosol Retrievals from Individual AVHRR Channels. Part I: Retrieval Algorithm and Transition from Dave to 6S Radiative Transfer Model

ALEXANDER IGNATOV* AND LARRY STOWE

NOAA/NESDIS/Office of Research and Applications/Climate Research and Applications Division, Washington, D.C.

(Manuscript received 29 December 2000, in final form 2 July 2001)

ABSTRACT

The present second-generation aerosol retrieval algorithm over oceans used at NOAA/National Environmental Satellite, Data, and Information Service (NESDIS) separately retrieves two values of aerosol optical depth, τ_1 and τ_2 , from Advanced Very High Resolution Radiometer (AVHRR) channels 1 and 2 centered at $\lambda_1 = 0.63$ (operational) and $\lambda_2 = 0.83 \mu\text{m}$ (experimental), respectively. From these, an effective Ångström exponent α , related to particle size, can be derived as $\alpha = -\ln(\tau_1/\tau_2)/\ln(\lambda_1/\lambda_2)$. The single-channel lookup tables, relating reflectance to optical depth in the retrievals, have been precalculated with the Dave (1973) scalar radiative transfer (RT) model. This first part of a two-part paper describes the retrieval algorithm, with emphasis on its RT modeling related elements, and documents the transition to the Second Simulation of the Satellite Signal in the Solar Spectrum (6S; 1997) RT model. The new 6S RT model has the capability to account for reflection from wind-roughened sea surface, offers a wide choice of flexible aerosol and gaseous absorption models, and allows easy convolution with the sensor's spectral response. The value of these new features for aerosol remote sensing from AVHRR is discussed in detail. The transition effect is quantified by directly applying the Dave- and 6S-based algorithms to four large datasets of NOAA-14 AVHRR measurements, collected between February 1998 and May 1999 over the latitudinal belt of 5° – 25°S . Statistics of the differences ($\delta\tau = \tau_{\text{Dave}} - \tau_{\text{6S}}$ and $\delta\alpha = \alpha_{\text{Dave}} - \alpha_{\text{6S}}$) are as follows: averages – $\langle\delta\tau_1\rangle < 1 \times 10^{-3}$, $\langle\delta\tau_2\rangle \approx -4 \times 10^{-3}$, and $\langle\delta\alpha\rangle \approx +8 \times 10^{-2}$; and standard deviations are $\sigma\tau_1 \sim 6 \times 10^{-3}$, $\sigma\tau_2 \sim 4 \times 10^{-3}$, and $\sigma\alpha \approx 9 \times 10^{-2}$. These are found to be well within a few percent of typical values of τ and α and their respective ranges of variability, thus ensuring a smooth transition and continuity in the operational aerosol retrieval. On the other hand, the 6S model provides a much more flexible RT modeling tool compared to the previously used Dave code.

1. Introduction

The Advanced Very High Resolution Radiometer (AVHRR/2) on board the National Oceanic and Atmospheric Administration (NOAA) polar orbiting satellites has five spectral channels centered at $\sim 0.63, 0.83, 3.7, 10.8,$ and $12 \mu\text{m}$ (Kidwell 1995). The AVHRR/3 sensor, flown on the NOAA-KLMN series of satellite (NOAA-15 and on) has an additional channel 3a in the midinfrared centered at $\sim 1.61 \mu\text{m}$. Channels 1, 2, and 3a, measuring reflected solar radiation, are useful for aerosol retrievals. The first-generation algorithm, a single-channel retrieval of aerosol optical depth in AVHRR channel 1, τ_1 , was implemented operationally with NOAA-11 data back in 1990 (Rao et al. 1989). The second-generation algorithm, an extended version of its

first generation, was implemented in December 1994 with the launch of NOAA-14 (Stowe et al. 1997). In addition to τ_1 , it is used to make an offline experimental single-channel retrieval of τ_2 from AVHRR channel 2, which later can be combined with τ_1 to estimate an effective Ångström exponent, $\alpha = -\ln(\tau_1/\tau_2)/\ln(\lambda_1/\lambda_2)$ (Ångström 1961, 1964, and references therein).¹ The Ångström exponent provides an indication of whether particles are big or small, which is critical to under-

* Currently a CIRA Visiting Scientist.

Corresponding author address: Dr. Alex Ignatov, NOAA/NESDIS/Office of Research and Applications/Climate Research and Applications Division, Washington, DC 20233.
E-mail: alex.ignatov@noaa.gov

¹ Note that reporting either a pair of (τ_1, τ_2) or (τ_1, α) is but a different way to present the two pieces of information from the two AVHRR/2 channels. Derivation of this set of parameters from AVHRR/2 was proposed by Ignatov et al. (1998). Ignatov and Stowe (2000) derive $[\tau_1, \tau_2$ (at $1.61 \mu\text{m}$), $\alpha]$ from the visible and infrared scanner (VIRS), a five-channel radiometer similar to the AVHRR but flown on board the Tropical Rainfall Measurement Mission satellite. The latter paper also provides extensive rationale to substantiate the use of the Ångström exponent as the retrieved aerosol size parameter. Work is under way on the third-generation algorithm, which will solve for τ and α simultaneously, using either channels 1 and 2 on AVHRR/2, or 1, 2, and 3a on AVHRR/3. This two-part study deals with individual channel retrievals only [see extensive discussion in Ignatov and Stowe (2000)], hence its title.

standing their radiative effects on climate (e.g., Lacis and Mishchenko 1995, and references therein).

Historically, both the first- and second-generation algorithms were implemented at the National Environmental Satellite, Data, and Information Service (NESDIS) with the Dave (1973) radiative transfer (RT) model, developed back in the early 1970s for ozone remote sensing from the Total Ozone Mapping Spectrometer (TOMS) [see also Dave (1978) and references therein]. The atmosphere is optically thick in the ultraviolet (UV), which calls for accurate accounting of multiple scattering effects in RT calculations. At the same time, modeling the bidirectional reflectance of the surface is less demanding in this spectral range, as it is largely masked by the opaque atmosphere. For TOMS ozone remote sensing, narrow quasi-monochromatic absorption bands are used. As a rule, radiative transfer in the ozone channels is influenced by aerosol as a secondary factor, which is considered a hindrance to be removed from the satellite measurement to rectify the ozone signal.

This specific application dictated the functionality and structure of the Dave code. Indeed, its RT engine has been long considered in the community a standard for multiple scattering monochromatic calculations in a multilayer atmosphere (e.g., Royer et al. 1988). Absorption by one gaseous component—ozone—was accurately parameterized, whereas all other absorbing constituents are missing from the original version of the code. The surface was simplistically characterized as being a purely diffuse (Lambertian) reflector.

Remote sensing of aerosol, however, articulates a different set of requirements. In particular, there is a greater need for a more sophisticated and flexible aerosol modeling, than may be considered sufficient for remote sensing of ozone. For example, many researchers now approximate aerosol microphysics with a bi- and even trimodal lognormal distribution (e.g., Tanre et al. 1997; Higurashi and Nakajima 1999), whereas the Dave code allows modeling of only one mode. Furthermore, the atmosphere, being more transparent in the red and near-infrared (R/NIR) than in the UV (due to a lower aerosol signal, and a much lower Rayleigh scattering contribution, which drop with wavelength as $-\lambda^{-1}$, and $-\lambda^{-4}$, respectively), can be treated with less accurate multiple scattering calculations. The surface, on the other hand, being seen through a more transparent atmosphere, requires a more adequate modeling of its bidirectional properties. AVHRR channel 1 is mainly influenced by ozone absorption, whereas channel 2 is strongly contaminated by water vapor absorption from the 0.94- μm band. Modeling of water vapor absorption with the Dave code is not straightforward. Finally, AVHRR channels are spectrally very wide, and their adequate modeling requires a convenient tool to convolute (integrate) the radiances over the satellite sensor's response.

Some of the above problems have been circum-

vented, to one extent or another, in the present Dave-based algorithm by a handful of homegrown improvements and additions to the code, developed over the years of its employment at NESDIS. As we work toward an improved aerosol retrieval algorithm at NESDIS, a more accurate and suitable RT code, which overcomes the limitations of the Dave code, should be used.

In this paper, the Second Simulation of the Satellite Signal in the Solar Spectrum (6S) RT model (Vermote et al. 1997a,b) is evaluated, and found to be well suited for the AVHRR aerosol retrievals. The 6S code uses successive orders of scattering, as opposed to the spherical harmonic, Gauss–Seidel iterative scheme employed in the Dave code. The accuracy of multiple scattering calculations with the 6S can be controlled by the user, at the expense of computing time (Vermote et al. 1997a,b). This is not expected to be crucial in the AVHRR spectral intervals, where radiative transfer is dominated by single scattering due to the fact that the Rayleigh scattering signal is small here, and aerosol optical depths over oceans are, typically, well below 1. Recall in this regard that a decoupled form of the single scattering approximation has been widely used to make an atmospheric correction for ocean color (e.g., Viollier et al. 1980; Gordon and Morel 1983; Guzzi et al. 1987) or land surface (e.g., Soufflet et al. 1991; Tanre et al. 1992) remote sensing, as well as for aerosol retrievals (e.g., Durkee et al. 1991; Breon and Deschamps 1993; Wagener et al. 1997) from AVHRR and AVHRR-like sensors. Therefore, the treatment of multiple scattering in 6S is expected to suffice for the accuracy requirements of our particular application. Results in section 6 support this expectation.

Aerosol modeling in 6S is very flexible, allowing for a few choices from either user-specified microphysical or standard composite models. In the microphysics menu, one can choose either a modified gamma, Junge power law, or a multimodal lognormal distribution (up to four modes). For a chosen microphysical model (for which a complex index of refraction must be specified at ten 6S reference wavelengths, from 0.4 to 3.75 μm), Mie calculations are run, and then used in the RT calculations. The six standard aerosol models (continental, maritime, urban, desert, biomass burning, and stratospheric) are those recommended by the World Meteorological Organization (World Climate Programme 1983, 1986). Note that the first three models in the list (continental, maritime, and urban) are composed of linear combinations (with certain weights) of the four built-in basic components (dustlike, water soluble, oceanic, and soot). Using user-specified weights, one can build a different aerosol model. Use of the standard models does not require running the 6S built-in Mie code. Results of Mie precalculations are already included in the body of 6S, and can be used by the user directly. Being less sophisticated than the relative humidity-dependent aerosol models of, for example, Shettle and Fenn (1979)

and d'Almeida et al. (1991), the above models nevertheless are useful for some aerosol-type related analyses. Furthermore, they assist in exploring the suite of microphysical models available in 6S, in particular, by providing a set of useful reference points for different, community consensus, aerosol types, and by objectively constraining their parameter ranges.

The 6S offers a wide choice of surface bidirectional reflection models, including a rough ocean surface, for which wind speed and direction are two input parameters. Also, it automatically accounts for absorption by major atmospheric gases, and has the capability to easily integrate over the satellite spectral response functions (including built-in spectral responses for many satellite sensors, such as AVHRR). The 6S computational efficiency compares very well with that of Dave, whereas the 6S interface is more user friendly, thus minimizing chances for making errors.

The 6S has also some (relatively minor) drawbacks, from the perspective of our particular application.

First, atmospheric absorption and scattering processes are decoupled in 6S, assuming all gaseous absorption to occur above the scattering layer.² This approximation works reasonably well in AVHRR channel 1, whose major absorber is ozone located at the altitude of ~18–20 km. But it becomes inadequate when an absorber is well mixed with the Rayleigh/aerosol scattering layer (parameter Δ deviates from 1 substantially). In AVHRR channel 2, the main gaseous absorber is water vapor, which has a strong absorption band centered at 0.94 μm , and is mostly concentrated in the lower troposphere (in terms of Soufflet et al. (1991) and Tanre et al. (1992), $\Delta \approx 0.5$, for average atmospheric conditions). When water vapor is located fully below the Rayleigh-aerosol scattering layer ($\Delta \rightarrow 0$), as is, for example, the case with African dust (Tanre et al. 1992), the 6S will lead to a substantial overestimate of the effect of water vapor on the upward radiance in AVHRR channel 2, whose radiance, as a result, will tend to be biased low. One way to adjust for this effect is to lower the water vapor amount in model calculations. This adjustment may require additional sensitivity study to the water vapor amount, and fine-tuning of this parameter in 6S RT calculations.

Second, 6S does not treat atmospheric sphericity. This problem is expected to be relatively minor in our applications, since limb observations, where the approximation of a plane parallel atmosphere fails, are excluded from the retrievals (presently, retrievals are made for solar zenith angles, $\theta_s < 70^\circ$, and view zenith angles,

$\theta_v < 60^\circ$, respectively).³ The technical difficulties associated with slant view/illumination angles larger than these, increase faster than the gains returned by the increase of aerosol signal there. Overall, the nonsphericity is not expected to be the major limiting factor, beyond restricting the domain of illumination and observation geometries useable for aerosol retrievals.

Third, the version of 6S available to the public (Verote et al. 1997a,b) and used in this study, is a scalar code, which may result in errors caused by the neglect of polarization effects. Work is under way to quantify the error associated with this scalar treatment, using other codes that have an “on-off” polarization switch. At present, the effect of polarization can be estimated using numerical results presented in Lacis et al. (1998), which quantified the effect for a purely Rayleigh atmosphere bounded below by an ocean surface roughened by wind. As the authors rightly state, the polarization effect on the intensity originates from second and higher orders of scattering in the atmosphere, which are mainly due to scattering by molecules rather than aerosol particles. Multiple scattering is very low in the R/NIR, as discussed above, and the Rayleigh optical depth is about three times lower in channel 1 (~0.06), an order of magnitude lower in channel 2 (~0.02), and more than two orders of magnitude lower in channel 3a (~0.001) than the smallest value of 0.2 considered by Lacis et al. (1998). Considering also the restricted domain of observation–illumination geometry used in the AVHRR retrievals, the maximum error in radiances due to the neglected polarization is estimated to be within 3%–5% in channel 1 at low aerosols. It is appreciably smaller in channels 2 and 3a, and gets progressively lower as aerosol optical depth increases.

Finally, the 6S does not allow modeling of the thermal emission, which limits its application, for example, for the analysis of effects of aerosol on the AVHRR brightness temperatures in channels 3, 4, and 5, and sea surface temperatures derived therefrom.

³ Increased aerosol signal at slant sun view angles make these geometries seemingly more attractive for aerosol remote sensing. Modeling accuracy, however, drops here, if a plane parallel approximation of the atmosphere is used. Also, at high zenith angles, model calculations are more sensitive to the uncertainties in the vertical and horizontal structure of the atmosphere. Additional difficulties may stem from the larger sensitivity of the upward radiances even to small uncertainties in the observation and illumination angles. This, in turn, leads not only to larger errors in the derived aerosol parameters from individual channels but also to misregistration between different channels, and as a result, to greater difficulties in their coherent use for cloud screening and aerosol retrievals. Our experience with AVHRR data suggests that these latter effects may be the major factors limiting the range of angles used, rather than nonsphericity or vertical structure of the atmosphere. Note also that the thresholds in θ_s and θ_v , which are expected to be the same from the reciprocity principle, differ due to the specifics of the cloud-screening algorithm used for operational aerosol retrievals. It will be further shown in section 7 of this paper that the retrieval lookup table introduces systematic errors in τ at $\theta_s > 60^\circ$, and therefore it is recommended that future retrievals be restricted to $\theta_s \leq 60^\circ$.

² This is not always the case. To take into account their coupling in the real atmosphere, Soufflet et al. (1991) and Tanre et al. (1992) introduced the so-called mixing ratio parameter Δ . The mixing parameter is defined in such a way that it is 0, when the absorber is fully below the scattering layer, and 1, when it is fully above. In 6S, according to this definition, $\Delta = 1$.

In this paper, the transition from Dave to 6S is evaluated empirically, and the associated effects in the aerosol products are quantified. Specifically, two lookup tables (LUTs), one based on Dave and the other on 6S, are constructed and applied to the four representative datasets from *NOAA-14 AVHRR/2*, which cover a period of more than a year. The analyses indicate that the transition from Dave to 6S has gone smoothly and predictably, providing continuity in the retrievals as well as a more flexible RT tool for developing algorithm enhancements.

In section 2, the retrieval algorithm is summarized, with particular emphasis on its RT modeling related elements. Wide spectral response of AVHRR channels, and its implication on aerosol retrievals, is discussed in great detail in section 3. Sea surface reflectance models in Dave and 6S are summarized in section 4. Section 5 describes the four datasets used in the study. The analysis of transition from Dave to 6S is done in section 6, and the retrieval algorithm induced errors are evaluated in section 7. Concluding remarks are given in section 8.

2. AVHRR second-generation aerosol retrieval algorithm

The second-generation AVHRR algorithm was described by Stowe et al. (1997). Ignatov and Stowe (2000) documented the Tropical Rainfall Measuring Mission (TRMM) VIRS version of this algorithm, which makes use of the two VIRS measurements centered at ~ 0.63 and ~ 1.61 μm (cf. with AVHRR, whose channels 1 and 3a (AVHRR/3 only) are near-identical to those of VIRS, and whose channel 2 is placed at ~ 0.83 μm). This section provides a summary of the algorithm, highlighting its AVHRR specific features and RT modeling related aspects. Stowe et al. (1997) and Ignatov and Stowe (2000) give more detail on its physical basis and premises, in a context of other alternate approaches proposed in the literature (e.g., Durkee et al. 1991, 2000; Tanre et al. 1997; Higurashi and Nakajima 1999; Mishchenko et al. 1999).

Aerosol retrievals are made in cloud-free conditions (McClain 1989) on the antisolar (backscattering) side of the orbit ($\varphi > 90^\circ$; φ is the relative azimuth), and outside of the sun glint area ($\gamma > 40^\circ$, γ is the glint angle defined so that $\gamma = 0$ when the satellite sensor is viewing precisely at the sun's reflected image on a flat ocean: $\varphi = 0^\circ$, $\theta_s = \theta_v$, where θ_s and θ_v are sun and view zenith angles, respectively). The algorithm for two reflectance channels derives two pieces of aerosol information, τ_1 and τ_2 , using two different single-channel lookup tables, LUT1 and LUT2, independently. The two LUTs are calculated for the same aerosol model, that is, a monomodal lognormal size distribution:

$$n(R) = \frac{dN}{dR} = \frac{1}{R \ln \sigma \sqrt{2\pi}} \exp\left(-\frac{\ln^2 \frac{R}{R_m}}{2 \ln^2 \sigma}\right), \quad (1)$$

with $R_m = 0.10$ μm ; and $\sigma = 2.03$; and a complex index of refraction, $n = 1.40 - 0.0i$. The aerosol phase function corresponding to this model, $P_{\text{oper}}(\chi)$, is shown in Figs. 1a,c. Nonaerosol atmospheric parameters (Rayleigh scattering and gaseous absorption), and oceanic reflectance used to calculate the LUTs, are described below.

Ignatov and Stowe (2000) have shown that application of this simplistic procedure to the VIRS data yields robust and reasonable τ_1 and τ_2 . Yet, the retrievals may be prone to errors, in particular, due to the assumption of a nonvariable aerosol phase function. Figures 1a–d show that in fact this assumption holds only approximately, and the variability of phase function in AVHRR channels 1 and 2 in backscatter may reach up to $\pm 30\%$ for a wide range of scattering geometry and even $\pm 50\%$, for selected scattering angles (cf. with Quenzel and Kaestner 1980; Kaufman 1993; Mishchenko et al. 1999). Ignatov and Stowe (2000) argued that this error in phase function translates into the same percent multiplicative error in the retrieved τ , when a fixed $P_{\text{oper}}(\chi)$ is used to interpret satellite measurements of aerosol path radiance (which is related to the product of an actual conservative phase function and actual optical depth). The ± 30 to $\pm 50\%$ uncertainty represents a worst-case scenario as it is derived from extreme aerosol models bracketing the range of variability around the globe, whereas typical errors are expected to be a few times less than these extreme estimates.

The derived τ are further combined to estimate an effective Ångström parameter α as⁴

$$\alpha = -\frac{\ln \frac{\tau_1}{\tau_2}}{\ln \frac{\lambda_1}{\lambda_2}} = \Lambda \ln \frac{\tau_1}{\tau_2}; \quad \Lambda = -\frac{1}{\ln \frac{\lambda_1}{\lambda_2}}. \quad (2)$$

Here, a spectral separation factor of the channels, Λ , is introduced. For the AVHRR channels 1 and 2 ($\lambda_1 = 0.63$, $\lambda_2 = 0.83$ μm), $\Lambda = 3.63$. For the aerosol model used in the retrievals, $\alpha_o = -\ln(\beta_1^{\text{ext}}/\beta_2^{\text{ext}})/\ln(\lambda_1/\lambda_2) \sim 0.94$, where β_i^{ext} is the Mie calculated volume extinction coefficient in channel i . [For AVHRR/3 channels 1 and 3a, $\Lambda \approx 1.07$ and $\alpha_o = 1.25$, see Ignatov and Stowe (2000)]. It might appear that using this model to retrieve τ_1 and τ_2 invariably results in $\alpha \equiv \alpha_o$, no matter what the real Ångström exponent is. However, Ignatov and Stowe (2000) argued that the retrieved α tends to be closer to the real α than to α_o . They have also shown

⁴ The Ångström exponent was estimated in this study whenever possible (τ_1 and $\tau_2 > 0$), whereas all numerical analyses of α were done only when both τ_1 and $\tau_2 > \tau_{\text{min}}$, to cut off the inaccurate α retrievals at low aerosols (Ignatov et al. 1998). The τ_{min} was set to 3×10^{-2} , to avoid indeterminacy and still allow analysis of the effect of τ_{min} on α retrievals at small τ (cf. Ignatov and Stowe 2000). This cutoff number should not be confused with a physically based threshold, which is yet to be determined from future theoretical and empirical analyses.

that a large part of the above error in τ cancels out while taking their ratio in the α calculation, due to the essentially coherent variations of the phase functions in the two VIRS channels. This coherence holds even better for the AVHRR channels 1 and 2, which are spectrally much closer to each other. Figures 1e–f documents this effect by showing natural logarithm of the ratio of the phase functions in the two channels, which typically falls within $\delta \ln(R) \sim \pm 0.1$ (except for some extreme cases when it may reach ± 0.2), which translates into a typical additive error of $\delta\alpha = \Lambda \delta \ln(R) \sim \pm 0.4$. Considering a typical range of α variability of $\delta\alpha \sim 2$, this error is considered tolerable in the second-generation algorithm.

3. Wide spectral response of AVHRR channels, and its handling in Dave and 6S

The Dave code performs monochromatic calculations at a given wavelength λ , with Rayleigh τ^R , aerosol τ , and ozone τ^{O_3} , optical depths being its input parameters (whose vertical distribution can be chosen according to one of the six standard atmospheres). Homegrown additions to the code, made in the late 1980s, allow one to take into account water vapor and carbon dioxide absorption, calculated for the AVHRR channels 1 and 2 using the LOWTRAN6 model (for midlatitude summer profiles, only).

Figure 2 shows the AVHRR spectral responses for the (afternoon) NOAA satellites used in creating a multiyear multisatellite AVHRR Pathfinder Atmosphere (PATMOS) dataset (Stowe et al. 2002). Among other implications, Fig. 2 suggests, in particular, that the choice of an effective wavelength as well as other input parameters, to represent the spectrally wide AVHRR channel with monochromatic Dave calculations, is not straightforward. It further suggests that all these parameters are not only channel, but also satellite-sensor specific. There are no built-in tools in the Dave code to handle all these convolutions over the sensor's spectral response, which need to be performed elsewhere, whereas the 6S code does them automatically using a suite of built-in subroutines and databases.

Even in case of accurate integration over the wide spectral response, interpretation of its results may not be straightforward. The problem of estimating τ_1 , τ_2 , and α from surface actinometric measurements with two wide spectral filters was discussed in great detail in the pioneering papers by Ångström (1961, 1964). He emphasized that "it is rather important that a certain simplicity of the technical procedure be maintained" when estimating α from integral measurements, and warned that one should be realistic about its expected accuracy. These considerations are still valid for the derivation of exactly the same set of aerosol parameters from AVHRR (note that AVHRR channels closely resemble those of the earlier surface actinometers). The satellite inversions involve more uncertainties, and

therefore are expected to be less accurate than ground-based measurements. In what follows, relevant definitions are given, and different aspects of this uncertainty are discussed.

a. Effective solar irradiance, F_{eff}

Table 1 lists values of the effective solar spectral irradiance F_{eff} for the AVHRR channels on board all NOAA satellites, calculated as

$$F_{\text{eff}} = \frac{\int F(\lambda)R(\lambda) d\lambda}{\int R(\lambda) d\lambda}. \quad (3)$$

Here, F ($\text{W m}^{-2} \mu\text{m}^{-1}$) is solar spectral irradiance [Neckel and Labs (1984), as tabulated in 6S], and R is the channel spectral response. Values of F_{eff} have been calculated here for completeness and illustrative purposes only. The actual conversion of satellite spectral radiance, L_i ($\text{W m}^{-2} \mu\text{m}^{-1} \text{sr}^{-1}$), into NOAA operational albedo units A_i , as $A_i = \pi L_i / F_{\text{eff},i}$ ($i = 1, 2, 3$ is channel number) uses data in Kidwell (1995), which compare with those listed in Table 1 typically within 0.1%–0.2%, and always within 1%.⁵

b. Effective wavelength, λ_{eff}

Table 1 lists the respective effective wavelengths of the channels λ_{eff} calculated as

$$\lambda_{\text{eff}} = \frac{\int \lambda F(\lambda)R(\lambda) d\lambda}{\int F(\lambda)R(\lambda) d\lambda}. \quad (4)$$

The weighting in Eq. (4) [also in Eq. (5)] is done only with respect to the solar energy spectral distribution at the top of the atmosphere within the spectral interval of the radiometer channel. However, the radiation changes its spectral structure after it is transmitted, or scattered by the atmosphere. In a purely molecular, single scattering atmosphere, $\lambda_{\text{eff}}^{(R)}$ could be defined through the equation $\tau_{\text{eff}}^R = \tau^R(\lambda_{\text{eff}}^{(R)})$. Here, τ_{eff}^R is calculated with Eq. (5) (discussed below), and $\tau^R(\lambda_{\text{eff}}^{(R)})$ (not shown in Table 2) can be estimated, for example, by Hansen and Travis' formula $\tau^R(\lambda) = (0.008569/\lambda^{-4})(1 + 0.0113/\lambda^{-2} + 0.00013/\lambda^{-4})$, as cited by Teillet (1990). Numerical estimates show that the respective $\lambda_{\text{eff}}^{(R)}$ are shift-

⁵ Table 3.3.2-2 of Kidwell (1995, 3–23) lists values of F (filtered solar irradiance, W m^{-2}) and W (effective width of channel, μm), from which F_{eff} is calculated as $F_{\text{eff}} = F/W$. Data for more recent satellites are available at <http://www2.ncdc.noaa.gov/docs/podug/index.htm>.

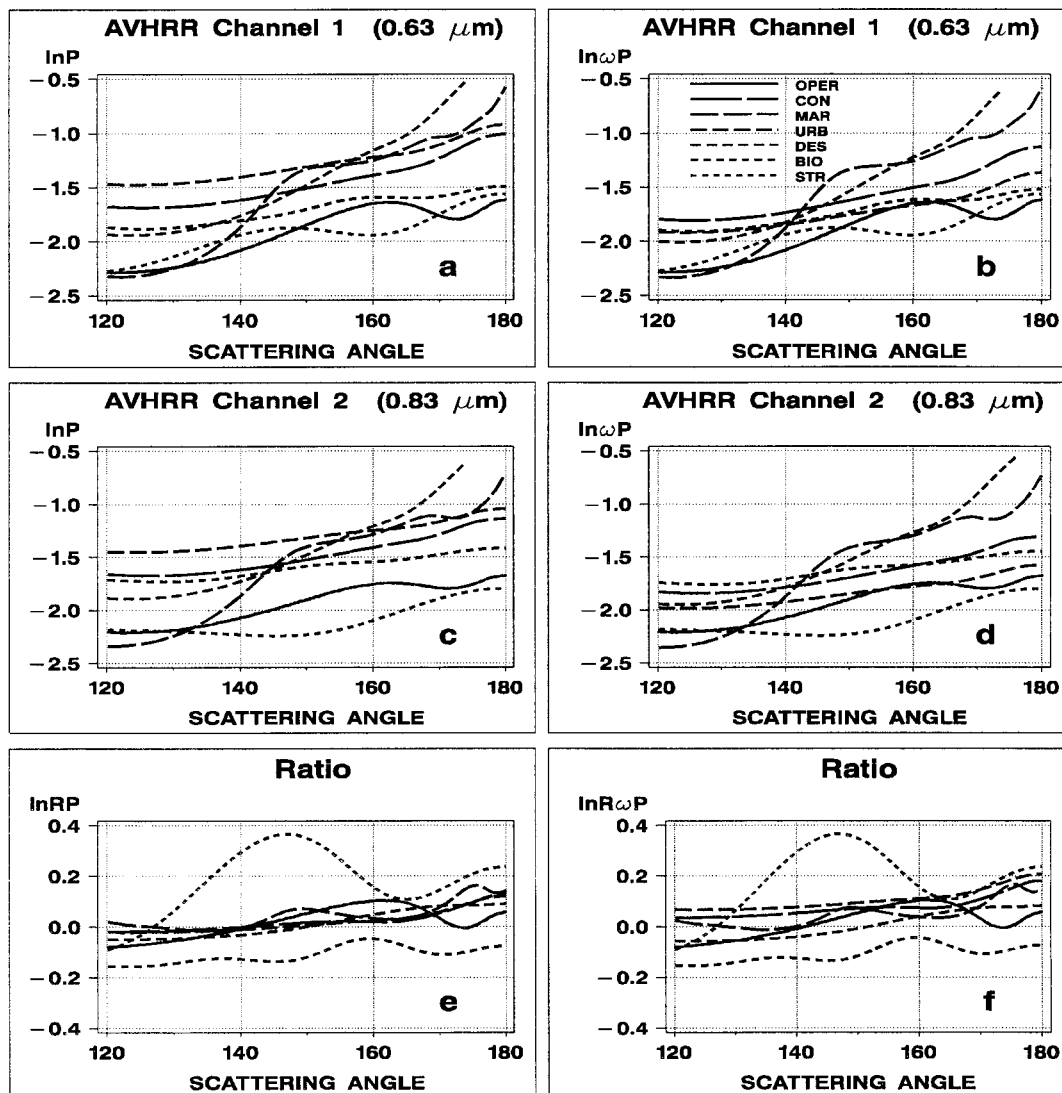


FIG. 1. The 6S model results for the six standard aerosol models [continental (CON), maritime (MAR), urban (URB), desert (DES), biomass burning (BIO), and stratospheric (STR)], and one microphysical model used in operational retrievals [monomodal lognormal size distribution with $n(R)$ defined in Eq. (1)] (OPER) in AVHRR channels 1 and 2 (0.63 and $0.83 \mu\text{m}$, respectively). The x axis is always scattering angle, χ . The y axis shows, on linear scale, (a) $\ln P$ —natural logarithm of the model phase functions in channel 1, $\ln[P_1(\chi)]$; (b) $\ln \omega P$ —natural logarithm of single scattering albedo (SSA) adjusted phase functions in channel 1, $\ln[\omega_1 P_1(\chi)]$; (c) same as (a) but in channel 2— $\ln P = \ln[P_2(\chi)]$; (d) same as (b) but in channel 2— $\ln \omega P = \ln[\omega_2 P_2(\chi)]$; (e) natural logarithms of ratios of phase functions— $\ln RP = \ln[P_1(\chi)/P_2(\chi)]$; (f) natural logarithms of ratios of the SSA-corrected phase functions— $\ln R\omega P = \ln[\{\omega_1 P_1(\chi)\}/\{\omega_2 P_2(\chi)\}]$. Note: the use of natural logarithm in (a)–(d) allows easy estimate of percent difference in phase functions. For instance, a 0.1 change in $\ln(X)$ (where $X = [P]$ or $X = [\omega P]$) corresponds to an $\sim 10\%$ difference in X , and subsequently, to a 10% error in τ . An equivalent error in α is estimated from (e) and (f) as $\delta\alpha \sim \Lambda \cdot \delta \ln R\omega P$, where $\Lambda \approx 3.63$ (see also section 2). This figure is fully similar to Fig. 1 in Ignatov and Stowe (2000) but for the AVHRR (0.63 and $0.83 \mu\text{m}$) rather than VIRS (0.63 and $1.61 \mu\text{m}$) channels.

ed toward shorter wavelength, with respect to $\lambda_{\text{eff}}^{\text{(R)}}$ listed in Table 1, by $\Delta\lambda_{\text{eff}}^{\text{(R)}} = 0.003\text{--}0.007$ and $0.015\text{--}0.019 \mu\text{m}$ in AVHRR channels 1 and 2, respectively (the dashes indicate ranges for different NOAA satellites in Table 1). The shift in channel 3a is negligible.

In a purely aerosol, single scattering atmosphere, the respective $\lambda_{\text{eff}}^{\text{(A)}}$ could be similarly defined by $\tau_{\text{eff}}^{\text{(A)}} = \tau^{\text{(A)}}(\lambda_{\text{eff}}^{\text{(A)}})$. Here, $\tau_{\text{eff}}^{\text{(A)}}$ is discussed later in the text, and

$\tau^{\text{(A)}}(\lambda_{\text{eff}}^{\text{(A)}})$ is estimated as $\tau(\lambda_{\text{eff}}^{\text{(A)}}) \sim \tau_0 \times (\lambda_{\text{eff}}^{\text{(A)}}/\lambda_0)^{-\alpha}$, α being the Ångström exponent, and τ_0 and λ_0 being reference values. The estimated shifts with respect to $\lambda_{\text{eff}}^{\text{(R)}}$ in Table 1 are $\Delta\lambda_{\text{eff}}^{\text{(A)}} = 0.001\text{--}0.003$ and $0.003\text{--}0.012 \mu\text{m}$ in channels 1 and 2 (the dashes here indicate range not only over different NOAA satellites but over the Ångström exponent range $0 \leq \alpha \leq 2$). Note that in all cases, $\Delta\lambda_{\text{eff}}^{\text{(A)}} < \Delta\lambda_{\text{eff}}^{\text{(R)}}$, implying that $\lambda_{\text{eff}}^{\text{(A)}}$ for different

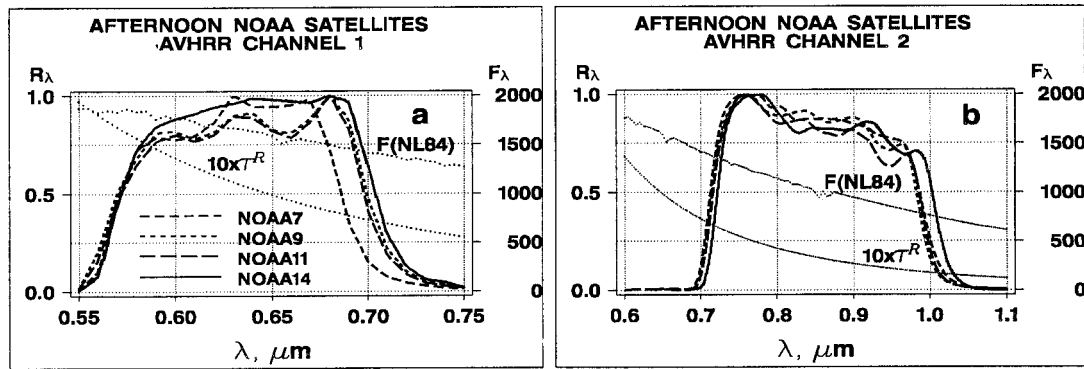


FIG. 2. Spectral response functions R [dimensionless; normalized to 1 at maximum; left y axis; shown only for afternoon NOAA satellites, used to produce the PATMOS dataset (Stowe et al. 2002)], Rayleigh optical depths τ^R (dimensionless; multiplied by a factor of 10; left y axis), and Neckel and Labs (1984) solar irradiance F ($\text{W m}^{-2} \mu\text{m}^{-1}$; right y axis) in AVHRR (a) channel 1 and (b) channel 2.

types of aerosols falls well between λ_{eff} listed in Table 1 and $\lambda_{\text{eff}}^{(R)}$. Mathematically, the Rayleigh case can be approximated by the Ångström formula, with $\alpha = +4$, whereas Eq. (4) follows from Eq. (5) if α is formally set to -1 . The Rayleigh case and the top-of-the-atmosphere case of Eq. (3) are formally equivalent to $\alpha = +4$, and $\alpha = -1$, respectively, and thus well bracket the aerosol domain corresponding to $0 \leq \alpha \leq 2$.

If one considers the additional effect of satellite-to-satellite variability, then λ_{eff} ranges from 0.621 to 0.640 μm in channel 1; from 0.811 to 0.844 μm in channel 2; and from 1.605 to 1.607 μm in channel 3a, depending upon satellite, definition of λ_{eff} , aerosol concentration, and variability in its Ångström exponent. Effectively, this demonstrates that $\lambda_1 = 0.63(\pm 0.010)$, $\lambda_2 = 0.83(\pm 0.017)$, and $\lambda_3 = 1.61(\pm 0.001)$ μm , can be used to refer to the central wavelengths of a generic AVHRR sensor. Taking into account approximate nature of the above estimates, the respective central wavelengths have been rounded off to the second decimal.

c. Choice of wavelengths to report the τ retrievals

Retrievals of τ may be reported at different wavelengths. The use of λ_{eff} seems to be the natural choice, but it depends upon its definition, and is NOAA satellite specific. The latter may pose an inconvenience when data from different satellites are combined in a consistent long-term climatic record, as is done, for instance, in the NOAA–National Aeronautics and Space Administration (NASA) AVHRR Pathfinder program (Stowe et al. 2002), or in a more recent NASA Global Aerosol Climatology Project (Mishchenko et al. 1999). In this study, a fixed set of AVHRR channel wavelengths, independent of satellite, was adopted as $\lambda_1 = 0.63$, $\lambda_2 = 0.83$, and $\lambda_3 = 1.61$ μm , which according to the previous analyses, are most representative of λ_{eff} for the majority of AVHRR sensors on different NOAA satellites.

Mishchenko et al. (1999) and Higurashi et al. (2000) use $\lambda_0 = 0.55$ and $\lambda_0 = 0.50$ μm , respectively, as a

TABLE 1. Effective central wavelengths and “solar constants” for different AVHRR/2 (NOAA-6–14), AVHRR/3 (NOAA-15, -16), and TRMM VIRS sensors [calculated according to Eqs. (3)–(4); $F(\lambda)$ —Neckel and Labs (1984), as tabulated in 6S]. Note: NOAA-13 is not present due to its short lifetime and lack of data records from its AVHRR/2 sensor. NOAA-14 was launched to replace it.

| | Channel 1 (0.63 μm) | | Channel 2 (0.83 μm) | | Channel 3A (1.61 μm) | |
|-----------|---|--|---|--|---|--|
| | λ_{eff} , μm | F_{eff} , $\text{W m}^{-2} \mu\text{m}^{-1}$ | λ_{eff} , μm | F_{eff} , $\text{W m}^{-2} \mu\text{m}^{-1}$ | λ_{eff} , μm | F_{eff} , $\text{W m}^{-2} \mu\text{m}^{-1}$ |
| NOAA-6 | 0.629 | 1657 | 0.834 | 1051 | — | — |
| NOAA-7 | 0.630 | 1651 | 0.834 | 1051 | — | — |
| NOAA-8 | 0.638 | 1619 | 0.830 | 1059 | — | — |
| NOAA-9 | 0.635 | 1631 | 0.833 | 1053 | — | — |
| NOAA-10 | 0.628 | 1658 | 0.836 | 1046 | — | — |
| NOAA-11 | 0.635 | 1631 | 0.832 | 1054 | — | — |
| NOAA-12 | 0.638 | 1621 | 0.834 | 1051 | — | — |
| NOAA-14 | 0.640 | 1610 | 0.844 | 1028 | — | — |
| NOAA-15 | 0.633 | 1648 | 0.840 | 1039 | 1.607 | 247.0 |
| NOAA-16 | 0.632 | 1649 | 0.843 | 1033 | 1.605 | 247.6 |
| TRMM VIRS | 0.624 | 1677 | — | — | 1.607 | 246.1 |

TABLE 2a. Channel 1 (0.63 μm) Rayleigh optical depth for different AVHRR/2 (NOAA-6-14), AVHRR/3 (NOAA15, -16), and TRMM VIRS sensors and standard atmospheres calculated according to Eq. (3). TROP—tropical, MLS—midlatitude summer, MLW—midlatitude winter, SS—subarctic summer, SW—subarctic winter, US62—standard U.S. (1962).

| | τ | TROP | MLS | MLW | SS | SW | US62 |
|-----------|------------------|--------|--------|--------|--------|--------|--------|
| NOAA-6 | Rayl | 0.0587 | 0.0586 | 0.0588 | 0.0583 | 0.0584 | 0.0585 |
| | H ₂ O | 0.0132 | 0.0099 | 0.0033 | 0.0074 | 0.0017 | 0.0052 |
| | O ₃ | 0.0212 | 0.0273 | 0.0340 | 0.0296 | 0.0411 | 0.0295 |
| | O ₂ | 0.0028 | 0.0028 | 0.0028 | 0.0028 | 0.0028 | 0.0028 |
| NOAA-7 | Rayl | 0.0584 | 0.0584 | 0.0585 | 0.0580 | 0.0582 | 0.0582 |
| | H ₂ O | 0.0134 | 0.0101 | 0.0034 | 0.0075 | 0.0017 | 0.0053 |
| | O ₃ | 0.0209 | 0.0269 | 0.0334 | 0.0291 | 0.0404 | 0.0289 |
| | O ₂ | 0.0032 | 0.0032 | 0.0031 | 0.0032 | 0.0031 | 0.0032 |
| NOAA-8 | Rayl | 0.0567 | 0.0566 | 0.0567 | 0.0562 | 0.0564 | 0.0564 |
| | H ₂ O | 0.0196 | 0.0154 | 0.0063 | 0.0121 | 0.0037 | 0.0092 |
| | O ₃ | 0.0199 | 0.0257 | 0.0320 | 0.0278 | 0.0386 | 0.0277 |
| | O ₂ | 0.0039 | 0.0039 | 0.0039 | 0.0039 | 0.0038 | 0.0039 |
| NOAA-9 | Rayl | 0.0571 | 0.0570 | 0.0571 | 0.0566 | 0.0568 | 0.0568 |
| | H ₂ O | 0.0160 | 0.0121 | 0.0041 | 0.0091 | 0.0021 | 0.0065 |
| | O ₃ | 0.0196 | 0.0252 | 0.0314 | 0.0273 | 0.0379 | 0.0272 |
| | O ₂ | 0.0059 | 0.0059 | 0.0058 | 0.0059 | 0.0058 | 0.0059 |
| NOAA-10 | Rayl | 0.0589 | 0.0589 | 0.0590 | 0.0585 | 0.0587 | 0.0587 |
| | H ₂ O | 0.0130 | 0.0097 | 0.0032 | 0.0072 | 0.0016 | 0.0051 |
| | O ₃ | 0.0213 | 0.0275 | 0.0342 | 0.0297 | 0.0413 | 0.0296 |
| | O ₂ | 0.0025 | 0.0025 | 0.0025 | 0.0025 | 0.0025 | 0.0025 |
| NOAA-11 | Rayl | 0.0569 | 0.0569 | 0.0570 | 0.0565 | 0.0567 | 0.0567 |
| | H ₂ O | 0.0155 | 0.0117 | 0.0040 | 0.0088 | 0.0020 | 0.0063 |
| | O ₃ | 0.0196 | 0.0253 | 0.0315 | 0.0274 | 0.0380 | 0.0273 |
| | O ₂ | 0.0059 | 0.0059 | 0.0059 | 0.0059 | 0.0058 | 0.0059 |
| NOAA-12 | Rayl | 0.0559 | 0.0559 | 0.0560 | 0.0555 | 0.0557 | 0.0557 |
| | H ₂ O | 0.0166 | 0.0126 | 0.0044 | 0.0096 | 0.0023 | 0.0069 |
| | O ₃ | 0.0194 | 0.0250 | 0.0312 | 0.0271 | 0.0376 | 0.0270 |
| | O ₂ | 0.0058 | 0.0058 | 0.0057 | 0.0057 | 0.0056 | 0.0057 |
| NOAA-14 | Rayl | 0.0555 | 0.0554 | 0.0555 | 0.0551 | 0.0552 | 0.0553 |
| | H ₂ O | 0.0188 | 0.0145 | 0.0053 | 0.0111 | 0.0029 | 0.0081 |
| | O ₃ | 0.0191 | 0.0245 | 0.0306 | 0.0266 | 0.0369 | 0.0264 |
| | O ₂ | 0.0059 | 0.0059 | 0.0058 | 0.0058 | 0.0057 | 0.0058 |
| NOAA-15 | Rayl | 0.0565 | 0.0564 | 0.0565 | 0.0561 | 0.0562 | 0.0562 |
| | H ₂ O | 0.0125 | 0.0093 | 0.0030 | 0.0069 | 0.0015 | 0.0048 |
| | O ₃ | 0.0212 | 0.0274 | 0.0341 | 0.0296 | 0.0411 | 0.0295 |
| | O ₂ | 0.0006 | 0.0006 | 0.0006 | 0.0006 | 0.0006 | 0.0006 |
| NOAA-16 | Rayl | 0.0568 | 0.0567 | 0.0568 | 0.0564 | 0.0565 | 0.0566 |
| | H ₂ O | 0.0129 | 0.0096 | 0.0031 | 0.0071 | 0.0016 | 0.0050 |
| | O ₃ | 0.0213 | 0.0274 | 0.0342 | 0.0297 | 0.0412 | 0.0296 |
| | O ₂ | 0.0007 | 0.0007 | 0.0007 | 0.0007 | 0.0007 | 0.0007 |
| TRMM VIRS | Rayl | 0.0599 | 0.0598 | 0.0599 | 0.0594 | 0.0596 | 0.0596 |
| | H ₂ O | 0.0132 | 0.0098 | 0.0032 | 0.0073 | 0.0016 | 0.0051 |
| | O ₃ | 0.0230 | 0.0297 | 0.0369 | 0.0321 | 0.0446 | 0.0320 |
| | O ₂ | 0.0004 | 0.0004 | 0.0004 | 0.0004 | 0.0004 | 0.0004 |

reference wavelength to report τ (the second reported parameter being an effective Ångström exponent). In both cases, the actual retrievals are extrapolated to λ_0 beyond the spectral interval in which the reflectance is measured, and therefore are subject to an additional component of error associated with the inferred aerosol model. An anonymous reviewer of this paper argued that “this reasoning seems to be a limitation of the approximate technique for the Ångström exponent retrieval adopted in this study. If a spectrally consistent aerosol model were used to retrieve τ and α , then the spectral interpolation would be exact and determined by the actual aerosol model, and the choice of wavelengths would be a matter of convenience.” Although it is generally true that α

derived in this study may be less accurate than that derived with simultaneous solution, the model inferred with any retrieval method is *never* fully accurate, due to the AVHRR radiometric uncertainties and to departures of retrieval algorithm assumptions from the actual retrieval conditions. In the presence of these uncertainties interpolation is generally more accurate than extrapolation. As, for example, Bevington and Robinson (1992) put it, “for optimum interpolation, the end points (x_o, x_n) should straddle the interpolation point x . The same formula can be used for extrapolating to values beyond the region of data, but the uncertainties in the validity of the approximation increase as x gets farther from the average of x_o and x_n .”

TABLE 2b. Same as Table 2a but for channel 2 (0.83 μm).

| | τ | TROP | MLS | MLW | SS | SW | US62 |
|---------|------------------|--------|--------|--------|--------|--------|--------|
| NOAA-6 | Rayl | 0.0199 | 0.0199 | 0.0199 | 0.0197 | 0.0198 | 0.0198 |
| | H ₂ O | 0.1425 | 0.1202 | 0.0601 | 0.1001 | 0.0378 | 0.0810 |
| | O ₃ | 0.0007 | 0.0009 | 0.0011 | 0.0010 | 0.0014 | 0.0010 |
| | O ₂ | 0.0159 | 0.0159 | 0.0155 | 0.0157 | 0.0152 | 0.0156 |
| NOAA-7 | Rayl | 0.0199 | 0.0199 | 0.0200 | 0.0198 | 0.0199 | 0.0199 |
| | H ₂ O | 0.1552 | 0.1313 | 0.0662 | 0.1096 | 0.0419 | 0.0889 |
| | O ₃ | 0.0008 | 0.0010 | 0.0012 | 0.0011 | 0.0015 | 0.0011 |
| | O ₂ | 0.0151 | 0.0150 | 0.0147 | 0.0148 | 0.0144 | 0.0148 |
| NOAA-8 | Rayl | 0.0203 | 0.0203 | 0.0203 | 0.0202 | 0.0202 | 0.0202 |
| | H ₂ O | 0.1424 | 0.1200 | 0.0599 | 0.0999 | 0.0376 | 0.0808 |
| | O ₃ | 0.0008 | 0.0011 | 0.0013 | 0.0011 | 0.0016 | 0.0011 |
| | O ₂ | 0.0163 | 0.0162 | 0.0158 | 0.0160 | 0.0156 | 0.0160 |
| NOAA-9 | Rayl | 0.0199 | 0.0199 | 0.0199 | 0.0198 | 0.0198 | 0.0198 |
| | H ₂ O | 0.1549 | 0.1309 | 0.0657 | 0.1092 | 0.0414 | 0.0885 |
| | O ₃ | 0.0007 | 0.0010 | 0.0012 | 0.0010 | 0.0014 | 0.0010 |
| | O ₂ | 0.0155 | 0.0155 | 0.0151 | 0.0153 | 0.0149 | 0.0152 |
| NOAA-10 | Rayl | 0.0195 | 0.0195 | 0.0195 | 0.0194 | 0.0194 | 0.0194 |
| | H ₂ O | 0.1469 | 0.1244 | 0.0630 | 0.1039 | 0.0399 | 0.0844 |
| | O ₃ | 0.0006 | 0.0008 | 0.0010 | 0.0009 | 0.0012 | 0.0009 |
| | O ₂ | 0.0166 | 0.0166 | 0.0162 | 0.0164 | 0.0159 | 0.0164 |
| NOAA-11 | Rayl | 0.0200 | 0.0200 | 0.0200 | 0.0198 | 0.0199 | 0.0199 |
| | H ₂ O | 0.1493 | 0.1260 | 0.0628 | 0.1048 | 0.0395 | 0.0848 |
| | O ₃ | 0.0008 | 0.0010 | 0.0012 | 0.0011 | 0.0015 | 0.0011 |
| | O ₂ | 0.0162 | 0.0161 | 0.0158 | 0.0159 | 0.0155 | 0.0159 |
| NOAA-12 | Rayl | 0.0198 | 0.0198 | 0.0198 | 0.0197 | 0.0197 | 0.0197 |
| | H ₂ O | 0.1482 | 0.1251 | 0.0626 | 0.1042 | 0.0394 | 0.0843 |
| | O ₃ | 0.0007 | 0.0009 | 0.0011 | 0.0010 | 0.0013 | 0.0010 |
| | O ₂ | 0.0127 | 0.0127 | 0.0122 | 0.0125 | 0.0119 | 0.0124 |
| NOAA-14 | Rayl | 0.0190 | 0.0189 | 0.0190 | 0.0188 | 0.0189 | 0.0189 |
| | H ₂ O | 0.1544 | 0.1308 | 0.0663 | 0.1093 | 0.0421 | 0.0889 |
| | O ₃ | 0.0006 | 0.0008 | 0.0009 | 0.0008 | 0.0011 | 0.0008 |
| | O ₂ | 0.0156 | 0.0155 | 0.0152 | 0.0153 | 0.0149 | 0.0153 |
| NOAA-15 | Rayl | 0.0189 | 0.0189 | 0.0190 | 0.0188 | 0.0189 | 0.0189 |
| | H ₂ O | 0.1604 | 0.1361 | 0.0694 | 0.1140 | 0.0441 | 0.0929 |
| | O ₃ | 0.0005 | 0.0006 | 0.0008 | 0.0007 | 0.0010 | 0.0007 |
| | O ₂ | 0.0140 | 0.0140 | 0.0137 | 0.0138 | 0.0134 | 0.0138 |
| NOAA-16 | Rayl | 0.0187 | 0.0187 | 0.0187 | 0.0186 | 0.0186 | 0.0187 |
| | H ₂ O | 0.1661 | 0.1411 | 0.0721 | 0.1182 | 0.0459 | 0.0964 |
| | O ₃ | 0.0005 | 0.0006 | 0.0008 | 0.0007 | 0.0009 | 0.0007 |
| | O ₂ | 0.0138 | 0.0138 | 0.0135 | 0.0136 | 0.0132 | 0.0136 |

Our rationale for using a set of wavelengths, maximally close to the three λ_{eff} , is the desire to minimize the component of error in τ , associated with extrapolation beyond the spectral interval, where actual retrievals are made. It is therefore left up to the user of the data to interpolate/extrapolate τ to other wavelengths, λ , using (τ_1, τ_2, τ_3) defined at $(\lambda_1, \lambda_2, \lambda_3)$ as reference points. The user must remember that this process is subject to the uncertainties described above.

d. Effective Rayleigh and gaseous optical depths (τ^R , τ^{O_3} , τ^{H_2O} , τ^{O_2} , τ^{CO_2} , τ^{CH_4})

These optical depths have been calculated from

$$\tau_{\text{eff}}^x = \frac{\int \tau^x(\lambda) F(\lambda) R(\lambda) d\lambda}{\int F(\lambda) R(\lambda) d\lambda}. \quad (5)$$

Here, $\tau^x(\lambda)$ is the spectral optical depth of a specie (Rayleigh τ^R , ozone τ^{O_3} , water vapor τ^{H_2O} , oxygen τ^{O_2} , carbon dioxide τ^{CO_2} , or methane τ^{CH_4} , respectively) as computed by the 6S RT code for different standard atmospheres. Table 2 shows Rayleigh optical depth and the optical depths of the five absorbing gaseous components in the AVHRR channels.⁶

Table 2 suggests that τ^R is atmospheric model and satellite specific. When the atmosphere changes from tropical to subarctic, even for the same satellite, τ^R ranges within $\delta\tau_1^R \sim \pm 2 \times 10^{-4}$ and $\delta\tau_2^R \sim \pm 1 \times 10^{-4}$ in

⁶ Gaseous concentrations for the TROP, MLS, MLW, SS, SW, and US62 standard atmospheres (for abbreviations, see Table 2 caption): O₂ (cm atm): 0.253, 0.324, 0.403, 0.350, 0.485, 0.349; O₃ (g cm⁻²): 5.42×10^{-4} , 6.95×10^{-4} , 8.64×10^{-4} , 7.50×10^{-4} , 10.40×10^{-4} , 7.48×10^{-4} ; and H₂O (g cm⁻²): 4.198, 2.982, 0.867, 2.108, 0.423, 1.439 (calculations by authors). For concentrations of uniformly mixed gases and for recalculation of cm atm units to g cm⁻², see McClatchey et al. (1971).

TABLE 2c. Same as Table 2a but for channel 3A (1.61 μm).

| | τ | TROP | MLS | MLW | SS | SW | US62 |
|-----------|------------------|--------|--------|--------|--------|--------|--------|
| NOAA-15 | Rayl | 0.0013 | 0.0013 | 0.0013 | 0.0013 | 0.0013 | 0.0013 |
| | H ₂ O | 0.0021 | 0.0015 | 0.0004 | 0.0010 | 0.0002 | 0.0007 |
| | CO ₂ | 0.0162 | 0.0162 | 0.0161 | 0.0161 | 0.0159 | 0.0161 |
| | CH ₄ | 0.0007 | 0.0007 | 0.0006 | 0.0006 | 0.0006 | 0.0006 |
| NOAA-16 | Rayl | 0.0013 | 0.0013 | 0.0013 | 0.0013 | 0.0013 | 0.0013 |
| | H ₂ O | 0.0023 | 0.0016 | 0.0005 | 0.0011 | 0.0002 | 0.0008 |
| | CO ₂ | 0.0162 | 0.0162 | 0.0161 | 0.0161 | 0.0159 | 0.0161 |
| | CH ₄ | 0.0005 | 0.0005 | 0.0004 | 0.0005 | 0.0004 | 0.0004 |
| TRMM VIRS | Rayl | 0.0013 | 0.0013 | 0.0013 | 0.0013 | 0.0013 | 0.0013 |
| | H ₂ O | 0.0029 | 0.0021 | 0.0007 | 0.0015 | 0.0004 | 0.0011 |
| | CO ₂ | 0.0153 | 0.0153 | 0.0152 | 0.0152 | 0.0150 | 0.0152 |
| | CH ₄ | 0.0018 | 0.0018 | 0.0017 | 0.0018 | 0.0017 | 0.0017 |

AVHRR channels 1 and 2, respectively. The satellite-to-satellite variability in τ^R is at least an order of magnitude greater ($\delta\tau_1^R \sim \pm 22 \times 10^{-4}$ and $\delta\tau_2^R \sim \pm 13 \times 10^{-4}$, respectively). (In channel 3a, the variability is negligible in either case.) These numbers should be scaled by a factor of ~ 5 to 10 [the ratio of Rayleigh and aerosol phase functions, which depends upon scattering geometry, and aerosol type; see, e.g., Ignatov and Stowe (2000)] to estimate the corresponding errors in the retrieved τ : $\delta\tau_1 \sim \pm(0.10-0.20) \times 10^{-2}$ and $\delta\tau_2 \sim \pm(0.05-0.10) \times 10^{-2}$ for the atmosphere-induced error for the same satellite, and $\delta\tau_1 \sim \pm(1.1-2.2) \times 10^{-2}$ and $\delta\tau_2 \sim \pm(0.65-1.30) \times 10^{-2}$ for the satellite-to-satellite error. The latter error is significant, and calls for the use of satellite-specific Rayleigh optical depths.

Similar analyses of gaseous optical depths τ^g in Table 2 show that the atmosphere-induced variability in τ^g is, at the very least, comparable with the satellite-induced variability, and even exceeds it a few times in either AVHRR channel. Its impact on the upwelling radiation, and on aerosol retrievals, is not easy to estimate, as it is strongly moderated by the relative vertical distribution of the absorbing layer (τ^g) with respect to the scattering layer ($\tau^R + \tau$). If the absorber is located below the scattering layer, just next to the black surface (the parameter Δ , defined in footnote 2, is $\Delta \sim 0$), its effect is negligible no matter what the τ^g is. The effect progressively increases with Δ , and reaches its maximum when $\Delta = 1$ [τ^g is fully above ($\tau^R + \tau$), as assumed in 6S].

At the present time, a midlatitude summer model (MLS) is assumed in the retrievals. This has two implications on the retrievals. First, on average, the effect of gaseous absorption on upward radiances is exaggerated with 6S for those gases well mixed with the molecular/aerosol layers (for instance, for water vapor, Δ is closer to 0.5 than to 1). As a result, the retrieved aerosol optical depth (in particular, τ_2) is overestimated. Second, unaccounted variations in gaseous absorption may cause spurious variability in aerosol retrievals, especially in AVHRR channel 2, which is strongly contaminated by water vapor absorption. Higurashi and Nakajima (1999) used real-time meteorological fields of

water vapor in their retrievals, but its vertical placement with respect to the scattering layer is still ambiguous. The effect of correction, and resulting improvement, still remain to be evaluated by means of sensitivity studies, similar to those recently undertaken by Ignatov (2002) for radiometric effects.

e. Effective aerosol optical depth, τ_{eff}

The τ_{eff} can be defined by substituting spectral aerosol optical depth, $\tau(\lambda)$, in place of $\tau^x(\lambda)$ in Eq. (5). A complication here stems from the fact that the spectral structure of $\tau(\lambda)$ is variable, unlike the fixed spectral structures in Rayleigh and gaseous absorber components. To estimate the magnitude of this dependence, recall that $\tau(\lambda)$ is customarily approximated as $\tau(\lambda) \sim \tau_o \times (\lambda/\lambda_o)^{-\alpha}$, $0 \leq \alpha \leq 2$. Integration of Eq. (5) was performed for different NOAA satellites, and for a few different values of α . The reference wavelengths of $\lambda_o = 0.63$, 0.83, and 1.61 μm were used for the three respective channels, and the same normalization factor of τ_o was conventionally adopted for different channels, for convenience [i.e., $\tau_i(\lambda_o) \equiv \tau_o$]. Performing integration, one obtains, for example, for NOAA-14 (the “worst-case scenario,” as λ_{eff} in both channels of NOAA-14 AVHRR/2, $\lambda_{1\text{eff}} = 0.640$ and $\lambda_{2\text{eff}} = 0.844$, deviate most substantially from λ_o): ($\tau_{1\text{eff}} = \tau_{2\text{eff}} = \tau_{3\text{eff}} = \tau_o$) for $\alpha = 0$; ($\tau_{1\text{eff}} = 0.981\tau_o$, $\tau_{2\text{eff}} = 0.977\tau_o$) for $\alpha = 1$; and ($\tau_{1\text{eff}} = 0.968\tau_o$, $\tau_{2\text{eff}} = 0.964\tau_o$) for $\alpha = 2$. As a result, the integral τ_{eff} may be lower than the monochromatic τ (the τ value at $\lambda_o = 0.63$ and 0.83 μm) by up to $\sim 3.2\%$ and 3.6%, respectively. The respective estimates for AVHRR/3 channel 3a yield difference of less than 0.6%.

f. Uncertainty in retrievals, resulting from uncertainties in τ_{eff} and λ_{eff}

In the present 6S retrievals, the more accurately estimated τ_{eff} is further scaled to estimate the monochromatic τ_1 and τ_2 at $\lambda_o = 0.63$ and 0.83 μm , using the prescribed operational model, having $\alpha = 0.94$ or $\alpha = 1.25$ for channels 1/2 or 1/3a, respectively, which is near the middle of the typical range in α . Thus the expected

uncertainties in the retrieved τ_i are within $\delta\tau_1 \sim \pm 1.6\%$, $\delta\tau_2 \sim \pm 1.8\%$, and $\delta\tau_3 \sim \pm 0.3\%$, respectively.

The retrieved Ångström exponent will also be in error as a result of the above uncertainties in the effective aerosol optical depths, and in the effective wavelengths $\delta\lambda_1 \sim \pm 0.010 \mu\text{m}$ (1.6%), $\delta\lambda_2 \sim \pm 0.017 \mu\text{m}$ (2.0%), $\delta\lambda_3 \sim \pm 0.001 \mu\text{m}$ (0.1%). Differentiating Eq. (2), and substituting $\delta\tau_1/\tau_1 \sim 1.6 \times 10^{-2}$, $\delta\tau_2/\tau_2 \sim 1.8 \times 10^{-2}$, $\delta\tau_3/\tau_3 \sim 0.3 \times 10^{-2}$; $\delta\lambda_1/\lambda_1 \sim 1.6 \times 10^{-2}$, $\delta\lambda_2/\lambda_2 \sim 2.0 \times 10^{-2}$, $\delta\lambda_3/\lambda_3 \sim 0.1 \times 10^{-2}$, one obtains that $\delta\alpha \sim \Lambda \times (\delta\tau_1/\tau_1 + \delta\tau_2/\tau_2 + \delta\lambda_1/\lambda_1 + \delta\lambda_2/\lambda_2) \sim 3.63 \times 7.0 \times 10^{-2} \sim \pm 0.25$ for α estimated from channels 1 and 2, and $\delta\alpha \sim \Lambda \times (\delta\tau_1/\tau_1 + \delta\tau_2/\tau_2 + \delta\lambda_3/\lambda_3 + \delta\lambda_3/\lambda_3) \sim 1.07 \times 3.6 \times 10^{-2} \sim \pm 0.04$ for α estimated from channels 1 and 3a.

Note that errors in τ_i , associated with wide AVHRR spectral response, are relatively small (do not exceed $\pm 2\%$ in channels 1 and 2, and $\pm 0.5\%$ in channel 3a). However, the error in the Ångström exponent may be up to ± 0.25 for channels 1 and 2, mainly due to the spectral closeness of these two channels (factor $\Lambda \sim 3.63$), whereas for channels 1 and 3a, it is substantially less (± 0.04).

4. Treatment of sea surface reflectance in Dave and 6S

a. Surface reflectance in Dave code

In the original Dave code, the atmosphere is bounded by a Lambertian reflector with surface reflectance ρ^s . This term is actually a sum of two contributions—foam reflectance (whitecaps, ρ_{wc}), and “underlight” (scattered radiation emerging from the sea water, ρ_{sw}) $\rho^s = \rho_{wc} + \rho_{sw}$. Ignatov et al. (1995) estimated ρ_{wc} and ρ_{sw} for the second-generation algorithm through careful analysis of the scientific literature. For whitecaps and underlight, Koepke’s (1984) model and empirical data by Morel and Prieur (1977) were used. For chlorophyll concentration (case 1 waters) and wind speed, typical of the open ocean, Ignatov et al. (1995) arrived at the following diffuse reflectances in AVHRR channels 1 and 2: $\rho_1^s = 2.0 \times 10^{-3}$ and $\rho_2^s = 0.5 \times 10^{-3}$. Below, the validity of these handmade estimates will be checked directly with 6S calculations, in which the Koepke’s (1984) and Morel (1988) models [the latter being based on empirical data by Morel and Prieur (1977)] have been implemented numerically.

For the second-generation algorithm, an additional “diffuse glint” term, $\Delta\rho_{gl}$, was added to the radiances, calculated with the Dave RT model:

$$\Delta\rho_{gl,i} = \frac{1}{4\mu_s\mu_v} [P_i^R(\gamma)\tau_i^R + P_i(\gamma)\tau_i][r_{f,i}(\mu_s) + r_{f,i}(\mu_v)]. \quad (6)$$

The simplistic formulation of Eq. (6), based on the decoupled form of the single scattering approximation to the RT equation, characterizes the bidirectional reflec-

tance from a flat ocean surface away from the direct glint area (Viollier et al. 1980; Gordon and Morel 1983). It represents two components of solar radiation that undergo only one act of scattering in the atmosphere, either before or after being reflected from a flat surface (the two terms in the second squared brackets, respectively). The first squared brackets represent the break-up of these into Rayleigh and aerosol contributions. In Eq. (6), ρ_i is the reflectance in channel i defined as $\rho_i = A_i/\mu_s$; $\mu_s = \cos(\theta_s)$, $\mu_v = \cos(\theta_v)$, where θ_s and θ_v are sun and view zenith angles, P^R and P are Rayleigh and aerosol phase functions, γ is the glint angle, and r_f is the Fresnel reflection coefficient for the ocean.

b. Surface reflectance in 6S model

In 6S, oceanic reflectance, $\rho_{os}(\theta_s, \theta_v, \phi, \lambda)$, is parameterized as follows (Vermote et al. 1997a,b):

$$\begin{aligned} \rho_{os}(\theta_s, \theta_v, \phi, \lambda) &= \rho_{wc}(\lambda) + (1 - \rho_{wc}) \times \rho_{sw}(\theta_s, \theta_v, \phi, \lambda) \\ &+ (1 - w) \times \rho_{gl}(\theta_s, \theta_v, \phi, \lambda). \end{aligned} \quad (7)$$

The first two terms on the right-hand side of Eq. (7) (due to whitecaps and underlight) are very small, and close to isotropic (diffuse Lambertian),⁷ and the third term is a bidirectional component (diffuse glint) explained above. The w parameter is the relative area covered with whitecaps [which is calculated in 6S according to Monahan and Muircheartaigh (1980) as $w = 2.95 \times 10^{-3} W^{3.52}$; W (m s^{-1}) is wind speed].

c. Diffuse (Lambertian) surface component in 6S

Taking into account the approximate character of whitecap and underlight models used in 6S, and the numerical estimates of footnote 7, we found it justified to make minor modifications to this part of the code, to

⁷ The foam reflectance above the surface is assumed to be Lambertian, as well as is the underlight just beneath the surface (level 0–). The latter deviates from isotropic after transition through a rough surface interface (level 0+) (Morel 1988). Special estimates with 6S have shown that this deviation depends upon illumination geometry (sun angle) and wind speed, but it is always within $\sim \pm 8\%$ for the full range of AVHRR sun view geometries, when wind speeds are $< 10 \text{ m s}^{-1}$. Accounting for this bidirectional effect may prove beneficial in the blue and green parts of spectrum, where a sizeable underlight signal, derived from satellite measurement by means of an atmospheric correction, is utilized for chlorophyll (“ocean color”) remote sensing. In the R/NIR AVHRR channels, the underlight signal is very low. Numerical estimates for AVHRR channel 1 show that over open ocean, it contributes about $\sim (0.5\text{--}2.0) \times 10^{-2}$ to τ_1 (about 5%–20% of typical τ_1 ; the range bracketed by dashes accounts for variable sun-view geometry and chlorophyll concentration). A $\pm 8\%$ error in it would thus result in a $\delta\tau_1 \sim (0.4\text{--}1.6) \times 10^{-3}$ error, well within 2% of typical τ_1 (and substantially less than $\delta\tau_1$ resulting from, e.g., chlorophyll natural variability, which is presently assumed non-variable in the retrievals). In channel 2, the underlight signal (and therefore associated errors $\delta\tau_2$) are at least an order of magnitude less than in channel 1 (e.g., Siegel et al. 2000).

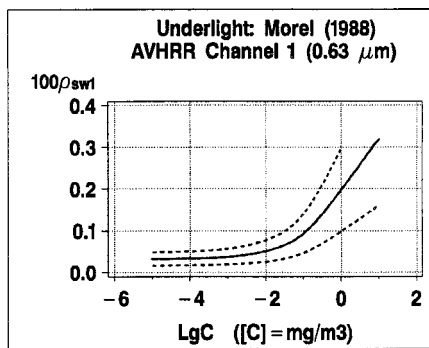


FIG. 3. Under light reflectance in AVHRR channel 1 as a function of chlorophyll concentration, C , mg l^{-1} [calculations using Morel (1988) model used in 6S]. Above $0.7 \mu\text{m}$ (and therefore in AVHRR channels 2 and 3a), the underlight signal is negligible. Solid lines, model prediction (Morel 1988; used in 6S); dotted lines, error bars (represented by a factor of 1.5: model predictions $\times 1.5^{-1}$ and $\times 1.5^{+1}$, respectively).

better fit our particular needs of aerosol retrievals at this time. The deviation of the underlight from an ideal Lambertian reflector was neglected, and the sum of two components, ρ_{wc} and ρ_{sw} , was approximated as a one-term diffuse reflectance, which can be fed as a direct input to 6S (in addition to the default option of calculating these components from chlorophyll concentration Chl and wind speed U).

Now, one needs to know the diffuse surface reflectance to be used as input to 6S. Figure 3 shows underlight reflectance, calculated as a function of chlorophyll

concentration according to Morel (1988) model (used in 6S), in AVHRR channel 1 only. For wavelengths above $0.7 \mu\text{m}$, and therefore for AVHRR channels 2 and 3a, Morel's (1988) model predicts a zero underlight. Figure 4 shows whitecaps reflectance as a function of wind speed, calculated from Koepke (1984) model. A recent model for whitecap reflectance by Frouin et al. (1996) suggests that the values of $\rho_{wc,1}$, $\rho_{wc,2}$, and $\rho_{wc,3}$ calculated according to Koepke (1984), must be scaled by factors of 0.95, 0.65, and 0.33, respectively (Frouin et al. 1996; Frouin 2000, personal communication). A recent study by Moore et al. (2000), carried out in a spectral range of $0.41\text{--}0.86 \mu\text{m}$, is in agreement with Frouin et al. (1996).

Note that these models have uncertainties. For the Koepke (1984) model, three major factors contribute to its uncertainty: fresh foam reflectance (0.22 ± 0.11), conversion factor to represent aged foam ($\sim 0.4 \pm 0.2$), and average foam coverage w [resulting from the uncertainty of the Monahan and Muircheartaigh (1980) equation, relating w to wind speed; see, e.g., their Fig. 1]. Part of these uncertainties may result from errors in the empirical data used to derive these parameterizations and approximations [e.g., both axes of Fig. 1 in Monahan and Muircheartaigh (1980) may be subject to measurement error], but this source of error is difficult to estimate. In an attempt to represent a typical rather than a worst-case scenario, a factor of 2 around the respective model predictions was used (model predictions $\times 2^{-1}$ and $\times 2^{+1}$, respectively). Same error bars are used for

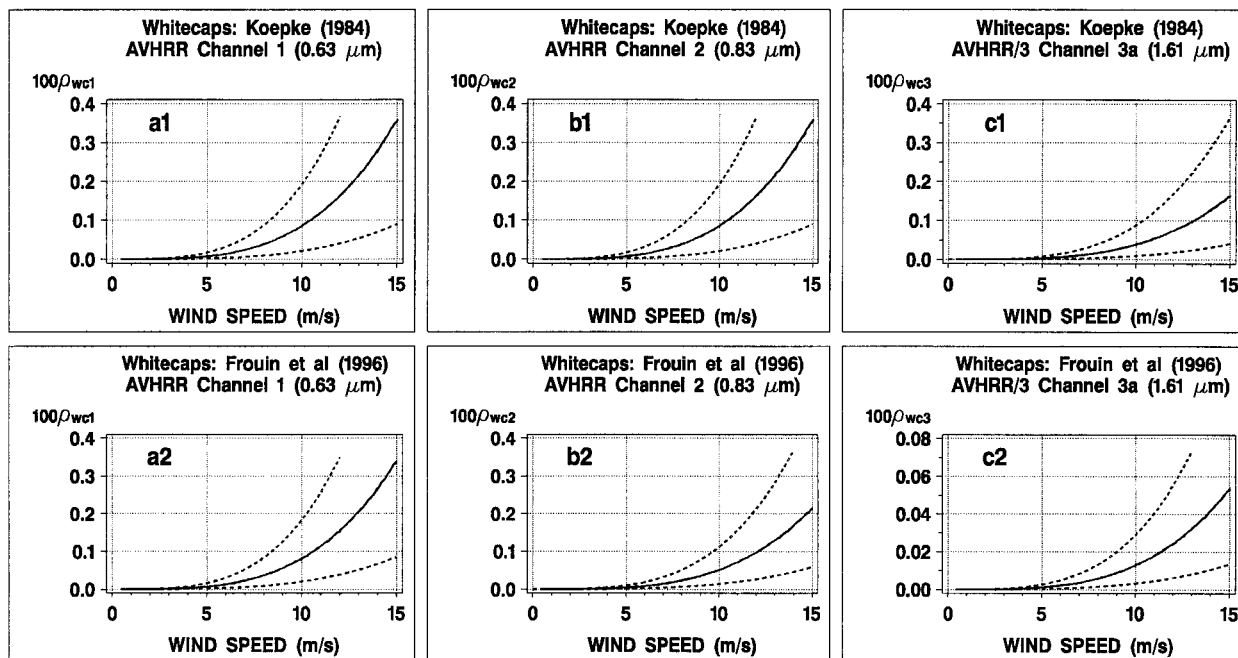


FIG. 4. Diffuse reflectance by whitecaps as a function of wind speed in AVHRR channels 1 (left) and 2 (middle), and AVHRR/3 channel 3a (right). (top, a1–c1) Koepke (1984) model (used in 6S); (bottom, a2–c2) Frouin et al. (1996) model. Solid lines, model predictions; dotted lines, error bars (represented by a factor of 2; model predictions $\times 2^{-1}$ and $\times 2^{+1}$, respectively).

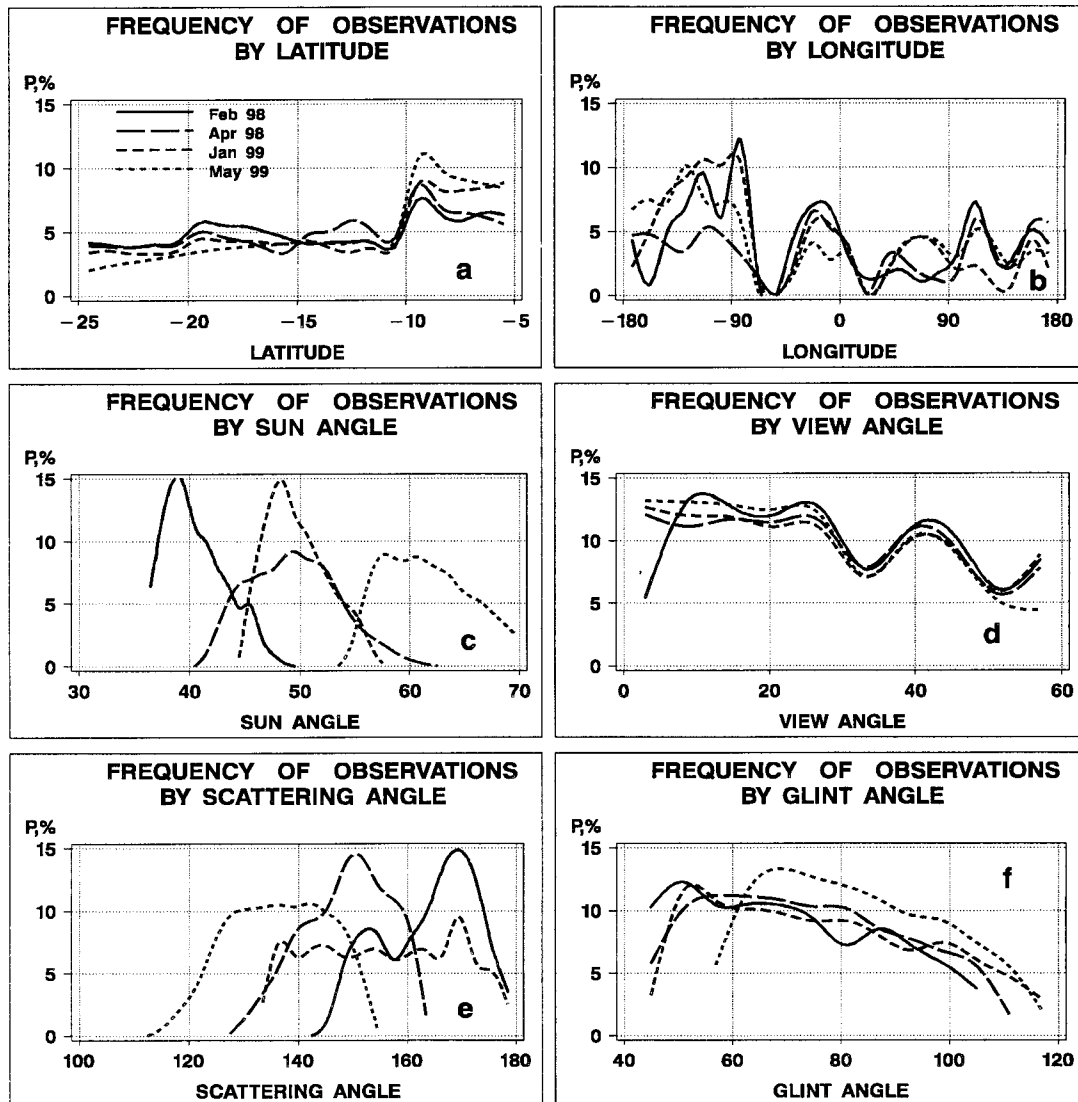


FIG. 5. Percent frequency distributions of observations in the four datasets used in this study (total number of observations is $N_1 = 67\,092$ in Feb98, $N_2 = 79\,269$ in Apr98, $N_3 = 101\,081$ in Jan99, and $N_4 = 108\,286$ in May99) by latitude φ (a), longitude λ (b), sun θ_s (c), view θ_v (d), scattering χ (e), and glint γ (f) angles. Bin sizes ($\Delta\varphi = 1^\circ$, $\Delta\lambda = 15^\circ$, $\Delta\theta_s = 1^\circ$, $\Delta\theta_v = 6^\circ$, $\Delta\chi = 3^\circ$, $\Delta\gamma = 3^\circ$) were chosen to normalize the maxima of the histograms at $\sim 15\%$, which was found to provide relatively smooth yet detailed structure of frequency distributions.

the Frouin et al. (1996) model. Morel (1988) gives no indication of error bars on the predictions from his model. Nevertheless, a factor of 1.5 is used (model predictions $\times 1.5^{-1}$ and $\times 1.5^{+1}$, respectively), to represent its uncertainty.

Figure 3 shows that for a typical chlorophyll concentration over open ocean of 0.05–0.5 mg/l (e.g., McClain et al. 1998), $\rho_{sw,1} \approx (1.2 \pm 1.0) \times 10^{-3}$, and $\rho_{sw,2} \approx \rho_{sw,3} \approx 0$. Figure 4 (bottom panels) suggests that for typical wind speed of $W \sim 5\text{--}8\text{ m s}^{-1}$, foam reflectance according to Frouin et al. (1996) is $\rho_{wc,1} \approx (0.22 \pm 0.22) \times 10^{-3}$, $\rho_{wc,2} \approx (0.15 \pm 0.15) \times 10^{-3}$, $\rho_{wc,3} \approx (0.04 \pm 0.04) \times 10^{-3}$. Summing the two components up, one arrives at the following results: $\rho_1^s =$

$(1.4 \pm 1.2) \times 10^{-3}$, $\rho_2^s = (0.15 \pm 0.15) \times 10^{-3}$, and $\rho_3^s = (0.04 \pm 0.04) \times 10^{-3}$ [cf. with values of $\rho_1^s = 2.0 \times 10^{-3}$, $\rho_2^s = 0.5 \times 10^{-3}$, and $\rho_3^s = 0.10 \times 10^{-3}$, respectively, recommended by Ignatov et al. (1995) based on Koepke's (1984) model]. Numerical estimates show that the effect of the systematic differences between these two estimates of ρ^s , $\Delta\rho_1^s = -0.6 \times 10^{-3}$, $\Delta\rho_2^s = -0.35 \times 10^{-3}$, and $\Delta\rho_3^s = -0.06 \times 10^{-3}$, on the derived τ is $\delta\tau_1 \sim +(0.2\text{--}0.8) \times 10^{-2}$, $\delta\tau_2 \sim +(0.1\text{--}0.5) \times 10^{-2}$, and $\delta\tau_3 \sim +(0.02\text{--}0.07) \times 10^{-2}$. The uncertainties in the diffuse surface reflectance, resulting from both the uncertainties in the model predictions and natural fluctuations in wind speed and chlorophyll concentration, are within $\pm 100\%$ of average model pre-

dictions. This causes random errors in retrieved τ of an order of $\delta\tau_1 \sim \pm(0.7-2.5) \times 10^{-2}$, $\delta\tau_2 \sim \pm(0.04-0.2) \times 10^{-2}$, and $\delta\tau_3 \sim \pm(0.01-0.05) \times 10^{-2}$.

Note that all the above estimates correspond to open ocean (case 1) waters. Over productive case 1, and coastal (case 2) waters the effect may be a few times larger—up to an order of magnitude and more [see, e.g., Siegel et al. (2000) and discussion in Ignatov and Stowe (2000)]. But the spectral tendency, by which the effect of diffuse surface reflectance is biggest in channel 1, and progressively decreases in channels 2 and 3a, is still valid. This is further discussed in Part II of this study.

d. Bidirectional component

The 6S uses an anisotropic Cox–Munk ocean surface bidirectional reflectance, with a slope distribution function, $P(W)$, represented by a Gram–Charlier series (Vermote et al. 1997b):

$$P = \frac{1}{2\pi\sigma_c\sigma_u} \exp\left(-\frac{\xi^2 + \eta^2}{2}\right) \times \left\{ 1 - \frac{1}{2}C_{21}(\xi^2 - 1) - \frac{1}{6}C_{03}(\eta^3 - \eta) + \frac{1}{24}C_{40}(\xi^4 - 6\xi^2 + 3) + \frac{1}{4}C_{22}(\xi^2 - 1)(\eta^2 - 1) + \frac{1}{24}C_{04}(\eta^4 - 6\eta^2 + 3) \right\}, \quad (8)$$

where

$$\begin{aligned} \sigma_c^2 &= 0.003 + 0.00192 \times W \pm 0.002 \\ \sigma_u^2 &= 0.000 + 0.00316 \times W \pm 0.004 \\ C_{21} &= 0.010 - 0.00860 \times W \pm 0.030 \\ C_{03} &= 0.040 - 0.0330 \times W \pm 0.120 \\ C_{40} &= 0.40 \pm 0.23 \quad C_{22} = 0.12 \pm 0.06 \\ C_{04} &= 0.23 \pm 0.41. \end{aligned} \quad (9)$$

Here, W is wind speed; $\xi = Z_c/\sigma_c$, $\eta = Z_u/\sigma_u$; Z_c and Z_u are wave slope components in crosswind and upwind directions, and σ_c and σ_u are their root-mean-squared deviations. Equations (8)–(9) are written in a system of orthogonal coordinates, referenced to wind direction, as described in Vermote et al. (1997b).

The anisotropic formulation of Eqs. (8)–(9), in which the crosswind and upwind directions are not equivalent, was first proposed by Cox and Munk (1954a,b, 1956). At the same time, Cox and Munk (1955) proposed a simplified isotropic treatment, with no reference to the wind direction. For some reason, it was this simplified

isotropic formulation that was later widely used in different remote sensing applications, including remote sensing of aerosol (e.g., Viollier et al. 1980; O'Brien and Mitchell 1988; Khattak et al. 1991; Breon 1993; Wagener et al. 1997; Mishchenko et al. 1999; Higurashi and Nakajima 1999).

The Cox–Munk surface model included in 6S offers a major improvement over the approximation described by Eq. (6) and used with the present second-generation algorithm. Additionally, its more sophisticated anisotropic wind formulation gives further opportunity to check the effect of the corresponding anisotropy in the surface roughness on the accuracy of aerosol retrievals, and thus better understand the applicability of the isotropic wind treatment used nowadays throughout the remote sensing community.

5. Data used in the study

This study uses the so called aerosol observations (AEROS) data, based on the operational sea surface temperature–aerosol cloud mask algorithm applied to 2×2 arrays of cloud-free global area coverage pixels (McClain 1989). For each cloud-free array, the mean geography (latitude and longitude), observation geometry (sun, view, and relative azimuth angles), radiometrically calibrated albedos (in channels 1 and 2), and brightness temperatures (in channels 3, 4, and 5) are produced, along with sea surface temperature and aerosol optical depth.

Four such datasets have been collected from NOAA-14 AVHRR/2, which all together span a period of more than a year, from February 1998 through May 1999. Each dataset contains AVHRR observations for a period of 9 to 14 consecutive days: 8–16 February 1998, 2–10 April 1998, 22 December 1998–4 January 1999, and 28 April–6 May 1999. These datasets are hereafter referred to as Feb98, Apr98, Jan99, and May99, respectively.

The calibration equation is used to convert output counts from AVHRR channels 1 and 2 into albedo [defined as spectral radiance in channel i , L_i ($W m^{-2} \mu m^{-1} sr^{-1}$) normalized to $F_{eff,i}$ ($W m^{-2} \mu m^{-1}$) as $A_i = \pi L_i / F_{eff,i}$]:

$$A_i = S_i(C - C_{0i}). \quad (10)$$

According to Rao and Chen (1996), the offsets are $C_{01} = C_{02} = 41$. The slopes, S_i , are different and change with time as

$$S_i = X_i + Y_i \times d, \quad (11)$$

where d is the elapsed time in orbit, expressed in days after launch (for NOAA-14, 30 December 1994).

The following coefficients have been used operationally:

| Before 8 Dec 1998 | After 8 Dec 1998 |
|-------------------------------|-------------------------------|
| $X_1 = 0.109$ | $X_1 = 0.1107$ |
| $Y_1 = 2.32 \times 10^{-5}$; | $Y_1 = 1.35 \times 10^{-5}$; |
| $X_2 = 0.129$ | $X_2 = 0.1343$ |
| $Y_2 = 3.73 \times 10^{-5}$; | $Y_2 = 1.33 \times 10^{-5}$. |

(12)

For the above four periods, $d_1 = 1141 \pm 4$; $d_2 = 1194 \pm 4$; $d_3 = 1460 \pm 6$; $d_4 = 1585 \pm 4$. Substituting these numbers in Eq. (12), one obtains the following values in channel 1: $S_1(d_1) = 0.1355$; $S_1(d_2) = 0.1367$; $S_1(d_3) = 0.1304$; $S_1(d_4) = 0.1321$; and in channel 2: $S_2(d_1) = 0.1716$; $S_2(d_2) = 0.1735$; $S_2(d_3) = 0.1537$; $S_2(d_4) = 0.1554$.

The first set of calibration coefficients, used before 8 December 1998, is based on Rao and Chen (1996). The second set of coefficients used thereafter is based on an internal memo by Dr. N. Rao (1998, personal communication). Therefore, the two subgroups of the four datasets (one subgroup including Feb98 and Apr98, and the other Jan99 and May99 datasets) have inconsistent calibration. Currently, yet another revision to the calibration formulas is under way (N. Rao 2000, personal communication). It was therefore decided not to revise/adjust the operational calibration of the data, for the present study. One should bear in mind, however, that the calibration issue, which is of little importance for the RT model comparison in the present study, may impact numerical results in the second part of this paper. A special sensitivity study has been recently completed by time of revision of this paper (Ignatov 2002), which provides a helpful guide to the future calibration adjustments as needed.⁸

Only data over the latitudinal belt of 5°–25°S have been considered. This area, according to our previous experience (cf. Husar et al. 1997), provides the cleanest atmosphere over oceans. The four datasets represent

space–time boxes (latitudinal belt of 5°–25°S, within 9–14 days) of AEROS data with numbers of observation of $N_1 = 67\,092$, $N_2 = 79\,269$, $N_3 = 101\,081$, and $N_4 = 108\,286$, respectively, and have different clustering in the subspace of sun-view geometry (see Fig. 5).

The data thus allow testing the accuracy of RT code transition (herein) and the performance of the algorithm [in Part II of this paper, Ignatov and Stowe (2002)] under a variety of different seasonal and angle conditions and a variety of different stages in the *NOAA-14* life cycle.

6. Transition from Dave to 6S

a. Mie schemes in Dave and 6S

First, the Mie part of 6S was tested against that of Dave (Ignatov 2000, unpublished manuscript). The scattering/extinction efficiencies and phase function are calculated in Mie theory via integration over particle radius size distribution. The difference between the Dave and 6S integration schemes is that in the former, an equal step in particle radius, Δr , is used, whereas in the latter, an equal logarithmic step is used as

$$\log\left(\frac{r + \Delta r}{r}\right) = \text{DRL} = 0.03, \quad (13)$$

with the $\text{DRL} = 3 \times 10^{-2}$ being a 6S built-in parameter. The Dave scheme requires that the equal-step parameter, Δr , be adjusted to the small particle end of the size distribution, which makes it excessively fine for the large-particle end. The more contemporary 6S-type numerical integration scheme is expected to be more computationally efficient, automatically providing comparable accuracy at both ends of the size distribution. This is due to the fact that the particles' size distribution is often approximated with a lognormal function.

Ignatov (2000, unpublished manuscript) has shown that the accuracy of the phase function calculation is more sensitive to this integration step size than is the accuracy of the extinction calculation. In order to achieve a $\sim 0.1\%$ accuracy in both phase function and extinction calculations over a realistic range of microphysical variability about the base microphysical model described in section 2, it was found that the DRL parameter in 6S needs to be reduced down to approximately $\text{DRL} = 2 \times 10^{-4}$. This value of integration step was used in all further calculations used in this paper.

b. Calculating radiances with 6S

Two new LUTs, for channels 1 and 2, respectively, have been constructed with 6S. The 6S built-in spectral response functions for *NOAA-14* AVHRR/2 were used. Surface diffuse reflectances were set to 2.0×10^{-3} , and 0.5×10^{-3} , as in the Dave LUTs. Wind speed was set to $W = 1 \text{ m s}^{-1}$, to more closely imitate the flat surface used with the Dave-based LUTs (smaller wind speeds have been avoided as they may result in instability of

⁸ Here, a preliminary illustration of the magnitude of this impact is given. In order to make the two subgroups radiometrically consistent in terms of Rao and Chen (1996), the albedos need to be raised by $\sim 9.6\%$ (in channel 1) and $\sim 19.3\%$ (in channel 2) in Jan99; and by $\sim 10.4\%$ and 21.1% , respectively, in May99. If their consistency is sought on the basis of N. Rao (1998, personal communication), the albedos should be lowered by 6.9% (channel 1) and 12.9% (channel 2) in Feb98; and by 7.2% (channel 1) and 13.5% (channel 2) in Apr98. The above estimates suggest that the calibration in the two groups of data is *inconsistent* by $\sim (6\text{--}10)\%$ and $\sim (13\text{--}20)\%$ in channels 1 and 2, respectively, whereas the data are *uncertain* within about $1/2$ that range, i.e., $\sim \pm(3\text{--}5)\%$ and $\sim \pm(6\text{--}10)\%$ in channels 1 and 2, respectively. [The uncertainty was estimated in anticipation that the future version of calibration will fall somewhere in between the Rao and Chen (1996) and N. Rao (1998, personal communication) versions.] Numerical estimates show that a $+5\%$ calibration error in channel 1 would raise τ_1 by $\delta\tau_1 \sim +(2\text{--}3) \times 10^{-2}$, and the same calibration error in channel 2 would raise τ_2 by $\delta\tau_2 \sim +(1\text{--}2) \times 10^{-2}$. Combining these two estimates together, one obtains that the two groups of data are *inconsistent* by $\delta\tau_1 \sim (3\text{--}6) \times 10^{-2}$ and $\delta\tau_2 \sim (3\text{--}8) \times 10^{-2}$, each being *uncertain* within $\delta\tau_1 \sim \pm(1\text{--}3) \times 10^{-2}$ and $\delta\tau_2 \sim \pm(1\text{--}4) \times 10^{-2}$, respectively.

the 6S numerical scheme, due to a singularity). Wind direction was set to 0; that is, the wind was assumed to blow in the scan plane. However, for such a low wind speed, this parameter does not matter. As in the Dave LUTs, the atmosphere was assumed to be mid latitude summer.

c. Comparison of 6S and Dave top-of-the-atmosphere (TOA) reflectances

Figure 6 shows the percent differences between 6S and Dave TOA reflectances. Reflectances from the look-up tables, which satisfy the retrieval restrictions [sun and view angles of $\theta_s, \theta_v = 0(6)60^\circ$; relative azimuth of $\varphi = 90(10)180^\circ$, and aerosol optical depth $\tau = 0(0.1)0.4$; the latter restriction is imposed because the vast majority of points in the four datasets have $\tau \leq 0.4$; $\gamma \geq 40^\circ$, $\varphi > 90^\circ$], are plotted versus scattering and glint angles. These two angles are chosen because they are felt to most clearly portray the differences in the atmospheric scattering and surface reflection, respectively.

The 6S–Dave percent differences in both channels are at their lowest (most negative) for a purely Rayleigh atmosphere (families of points closest to the x axes in Fig. 6), and increase with τ . In channel 1, they remain typically within a few percent. In channel 2, Dave aerosol radiances are systematically biased high with respect to 6S, and the respective percent differences are higher than in channel 1. Depressed 6S reflectances in this channel are related to the specifics of accounting for gaseous absorption in 6S (in this particular case, it is water vapor), which is assumed to be fully above the Rayleigh-aerosol scattering layer. This feature of 6S has already been discussed in sections 1 and 3a and indicates that the 6S calculations may require some future adjustments to the concentrations of the absorbers, to represent actual radiative transfer in the atmosphere more realistically. This adjustment is not attempted in this paper, in which fixed midlatitude summer profiles are used for each gaseous component, and will be explored elsewhere. As a result of this low bias in channel 2 reflectances, the retrievals of aerosol optical depth in this channel with 6S LUTs are expected to be biased somewhat high.

In both channels, systematic angular bias is more noticeable for glint angle, the Dave reflectances being biased progressively high as one approaches the cutoff glint angle of $\gamma = 40^\circ$, adopted in the present algorithm. This may be due to the fact that a homegrown addition to the Dave code to treat the diffuse glint correction in a simplified manner based on a decoupled form of the single-scattering approximation (as described in section 4a) overestimates the contribution from this term compared to its more accurate treatment in 6S.

Note that Fig. 6 can only be used to give a very rough idea of the effect of changing RT models, as it is unclear what realistic proportion of points with different geometries and aerosol conditions actually is in the

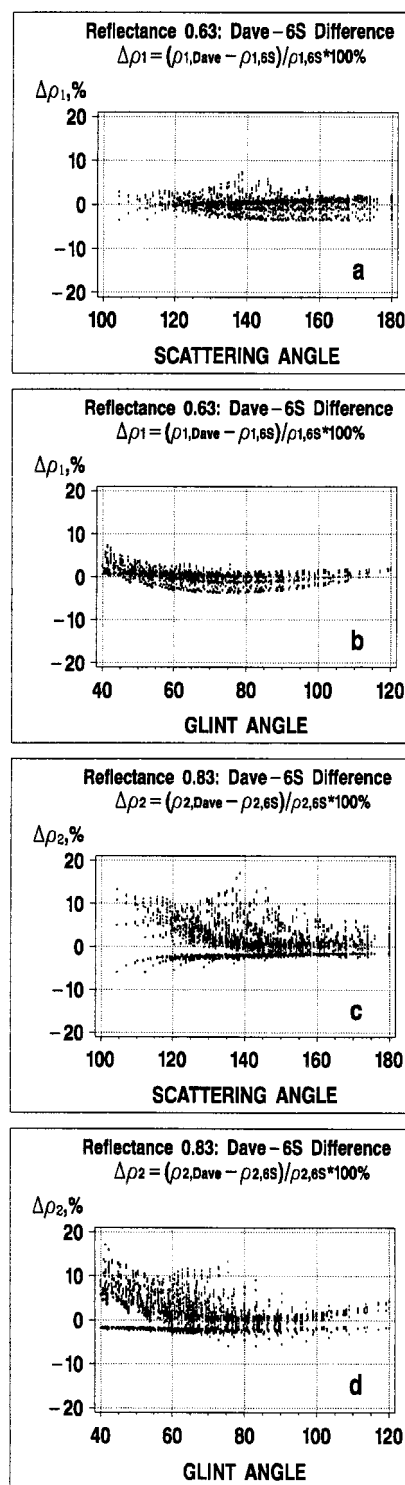


FIG. 6. Percent difference between Dave and 6S reflectances in AVHRR channels 1 (a)–(b) and 2 (c)–(d) vs scattering (a), (c) and glint (b), (d) angles.

AVHRR retrievals. Thus, to estimate the impact of changing the RT model on the aerosol retrievals more realistically, the actual geometrical retrieval conditions (presented in Fig. 5), and aerosol optical depth frequency distributions (considered in the second part of this study) in the four datasets must be taken into account. Below, this is done by comparing actual retrievals with the two models.

d. Comparison of 6S and Dave retrievals

Figure 7 shows scattergrams of the Dave-based retrievals of τ_1 , τ_2 , and α against respective 6S-based retrievals of these parameters. They are practically identical at low aerosols, but begin to diverge as aerosol amount increases, consistent with the reflectance differences in Fig. 6. (Note that the inconsistent calibrations between the two subgroups of the four datasets affect mostly the low-end τ retrievals, but this has little impact when comparing 6S and Dave.)

Figure 8 shows histograms of their differences and statistics of the comparisons (mean, root-mean-squared deviation, minimum, and maximum differences). The retrieved optical depths with the two RT models are typically within ± 0.02 of each other in both channels. In channel 1, the bias in τ is negligible ($\langle \delta\tau_1 \rangle < 1 \times 10^{-3}$); in channel 2, the 6S-derived τ_2 are biased high, in qualitative agreement with the reflectance analysis, by $\langle \delta\tau_2 \rangle \approx 4 \times 10^{-3}$. Mean bias in the derived Ångström exponent is $\langle \delta\alpha \rangle \approx +8 \times 10^{-2}$. Random (standard deviation) differences are about $\sigma\tau_1 \sim 6 \times 10^{-3}$ in channel 1, and $\sigma\tau_2 \sim 4 \times 10^{-3}$ in channel 2, and $\sigma\alpha \approx 9 \times 10^{-2}$ in the Ångström exponent.

It is interesting that a small bias in channel 2 results in a noticeable bias in the Ångström exponent. The high sensitivity of this differential aerosol parameter is further illustrated in Fig. 9, which shows the “Dave – 6S” Ångström exponent difference, $\Delta\alpha = \alpha_D - \alpha_{6S}$, as a function of aerosol optical depth in channel 1. Systematic components of $\Delta\tau_2$ (and, to a lesser extent, in $\Delta\tau_1$) result in a pronounced $1/\tau$ -type trend in $\Delta\alpha$, whereas their random components contribute to a pronounced scatter around this $1/\tau$ -trend. Note that the May99 dataset reveals higher noise in $\Delta\alpha$, especially at low τ . A lower τ in this dataset compared to the other three (see discussion in the next section) may tend to amplify the differences between the 6S and Dave Ångström exponent retrievals. The differences themselves may be larger here, too, because the diffuse glint correction added to the Dave code is expected to perform progressively less accurately as solar zenith angle increases.

Overall, the magnitude of uncertainty in τ , resulting from the conversion from one RT code to another, appears acceptable for aerosol retrievals. For example, it is well within the MODIS goal: retrieving τ to an accuracy of $\pm 0.05 \pm 0.05\tau$ (Tanre et al. 1997). Relative differences in the Ångström exponent are larger, but still

can be tolerated considering other sources of its uncertainty (see Part II of this study for details).

7. Errors in τ caused by the retrieval procedure (lookup table interpolation scheme)

Changing RT models leads to examining the performance of elements of the retrieval algorithm, other than the RT code, such as the numerical scheme used in the retrieval algorithm. At present, LUTs are customarily used for aerosol retrievals (e.g., Tanre et al. 1997; Higurashi and Nakajima 1999), the retrieved value being estimated by a multidimensional interpolation between its rows and columns. The NOAA/NESDIS second-generation algorithm inherited the numerical retrieval scheme from the first-generation algorithm (Rao et al. 1989). The LUT is a four-dimensional matrix of pre-calculated top-of-the-atmosphere albedos: 15 sun zenith angles [$(\theta_s = 0(6)84^\circ)$] \times 15 view zenith angles [$(\theta_v = 0(6)84^\circ)$] \times 19 relative azimuth angles [$(\varphi = 0(10)180^\circ)$] \times 7 aerosol optical depths ($\tau = 0, 0.15, 0.30, 0.60, 0.90, 1.20, \text{ and } 1.50$). [Note that LUTs of a similar structure are presently used for moderate resolution imaging spectroradiometer (MODIS) retrievals (Tanre et al. 1997).] The interpolation is second-degree Lagrangian in a four-dimensional space.

Accuracy of this retrieval procedure has been examined by means of the following numerical experiment. For all four datasets described above, the measured albedos have been replaced by theoretically calculated values, for the exact sun-view geometry available from the data. Aerosol optical depth, τ_m , needed as input for the albedo calculations, was modeled as belonging to a random sample with a lognormal probability distribution function with a geometrical mean, $\tau_g = 0.15$, and standard deviation, $\mu = 1.5$ in both channels (for definitions, and validity of this approach in general, and its specific parameters in particular, see second part of this study). The set of atmospheric and oceanic surface parameters, used for modeling, is that used in the second-generation algorithm, as described above. The operational retrieval procedure was then applied to invert the calculated albedos back to “estimated” aerosol optical depths, τ_e , using LUTs whose parameters are fully consistent with the parameters in the calculation. The difference between the “modeled” τ_m , and “estimated” τ_e , was then calculated as $\Delta\tau = \tau_e - \tau_m$ in the first two AVHRR channels. Typically, $\Delta\tau_i$, are close to zero, which is expected if the retrieval procedure performs adequately. However, retrievals at high solar zenith angles were found to be biased low. Figure 10 plots $\Delta\tau_1$ and $\Delta\tau_2$ as a function of sun angle for the May99 dataset. (The three other datasets have very few observations with $\theta_s > 60^\circ$ (cf. Fig. 5c), and therefore are not shown here). Negative bias starts developing beyond $\theta_s = 60^\circ$, and reaches $\Delta\tau_1 = -0.04$ and $\Delta\tau_2 = -0.02$ in channels 1 and 2 at $\theta_s = 70^\circ$, on average. (Recall that a similar feature should have been

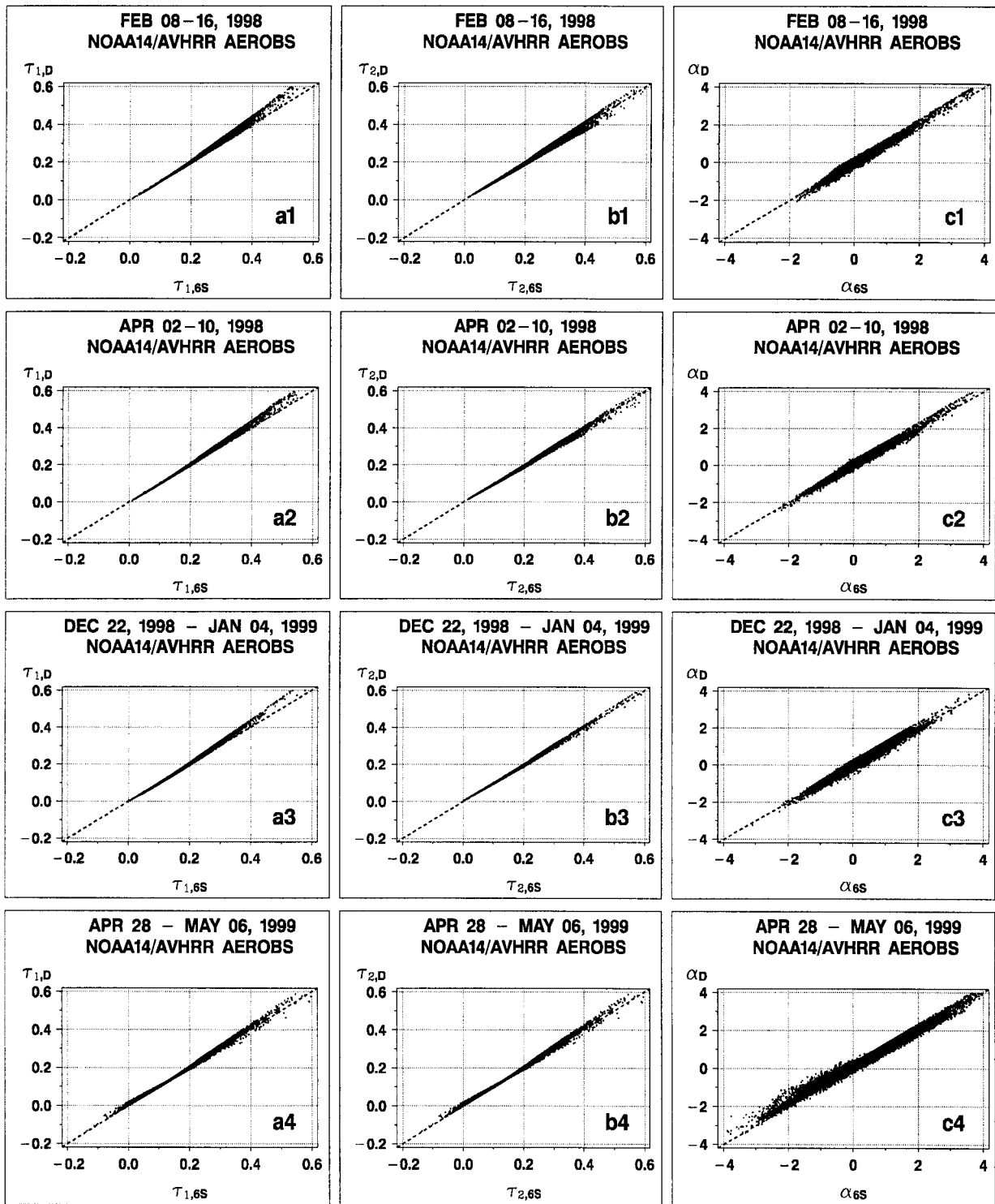


FIG. 7. Scattergrams of τ_1 (a), τ_2 (b), and α (c) derived using Dave vs those derived using the 6S code, for the four different datasets: Feb98 (dataset 1); Apr98 (dataset 2); Jan99 (dataset 3); May99 (dataset 4).

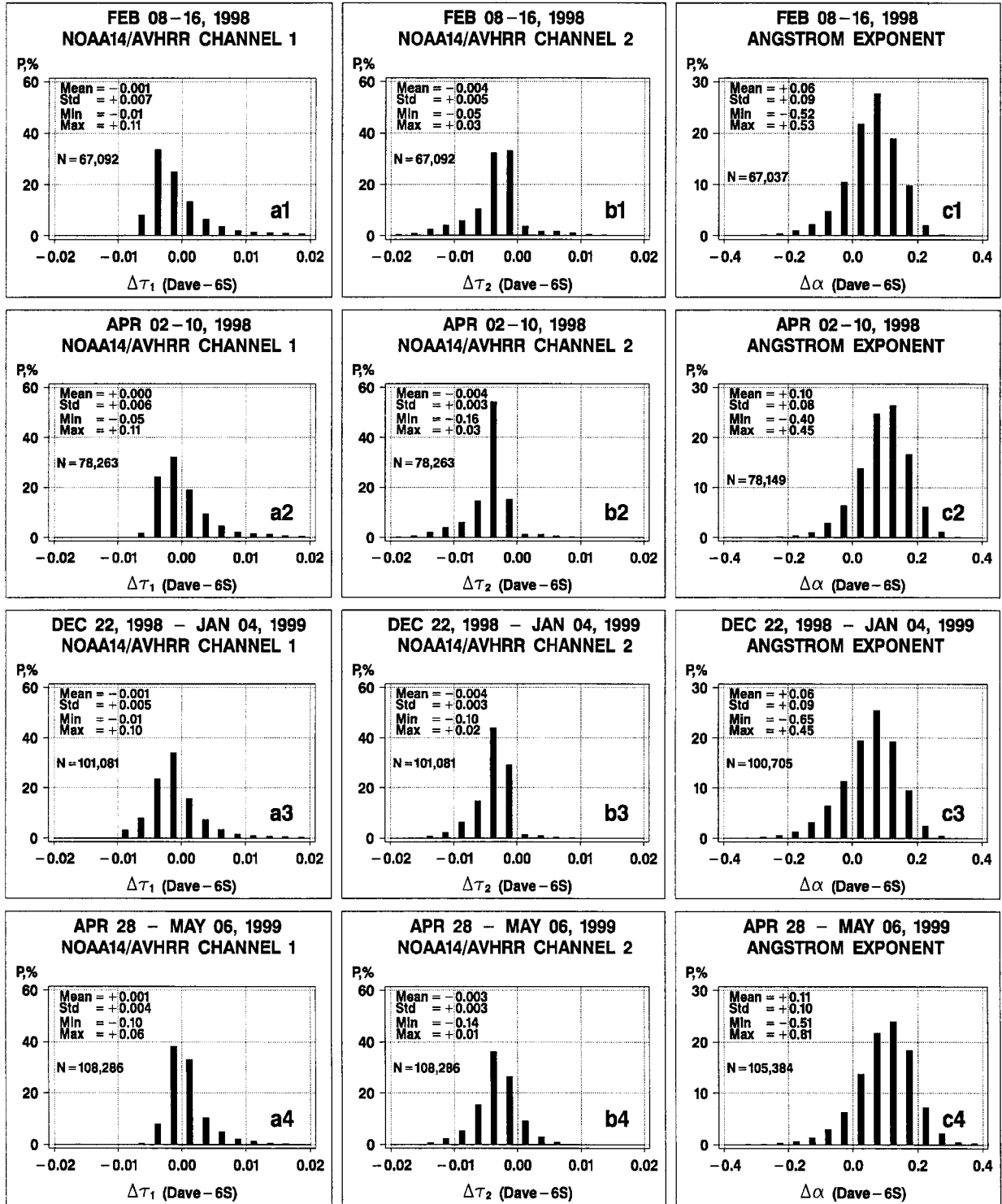


FIG. 8. Histograms of Dave - 6S differences for τ_1 (a), τ_2 (b), and α (c) for the four different datasets: Feb98 (dataset 1), Apr98 (dataset 2), Jan99 (dataset 3), May99 (dataset 4). (Note: statistics for α are calculated for $\tau_1 \tau_2 > 0.03$ only.)

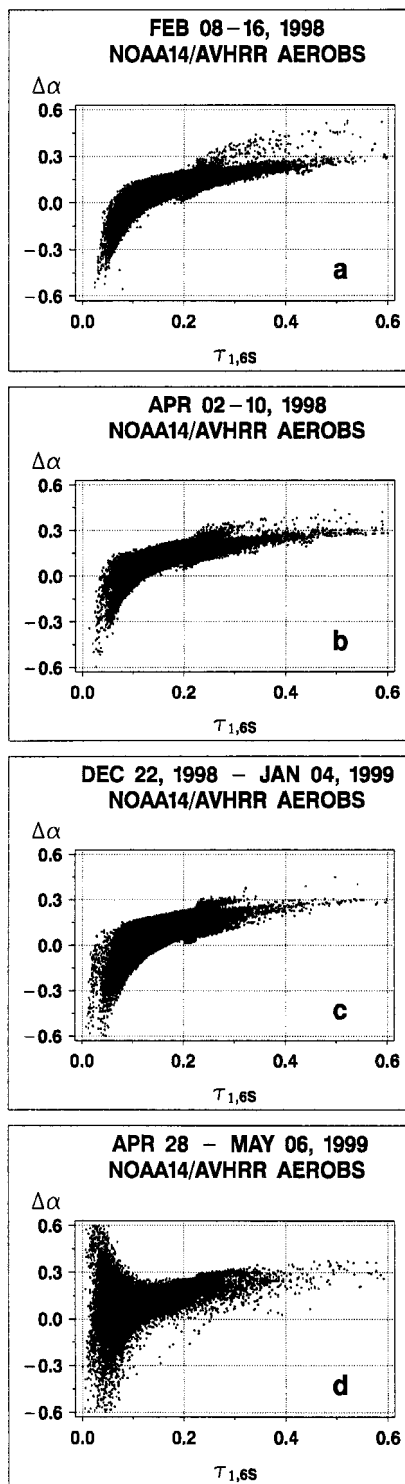


FIG. 9. Scattergrams of Dave $-6S$ differences in the Ångström exponent, $\Delta\alpha = \alpha_D - \alpha_{6S}$, as a function of aerosol optical depth in channel 1, for the four different datasets: Feb98 (a), Apr98 (b), Jan99 (c), May99 (d).

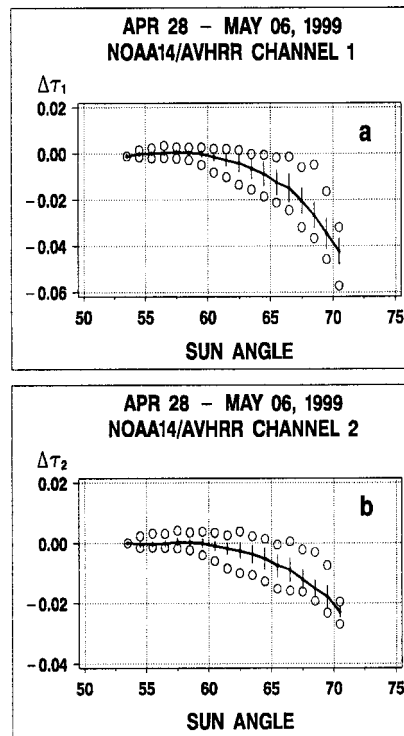


FIG. 10. Errors in aerosol optical depth in AVHRR channels 1 (a), $\Delta\tau_1$, and 2 (b), $\Delta\tau_2$, induced by the retrieval procedure, as a function of solar zenith angle, for the May99 dataset. Solid line, average $\Delta\tau_i$; vertical bars, standard deviation $\sigma_{\Delta\tau_i}$; open circles, $\min(\Delta\tau_i)$ and $\max(\Delta\tau_i)$.

observed, due to the reciprocity principle, at slant view angles, which may go as high as 68° for the AVHRR. However, angles with $\theta_v > 60^\circ$ are not present in the retrievals, due to the specifics of the cloud mask used in the operations, described in footnote 3.) The channel 3a ($1.61 \mu\text{m}$) data from AVHRR/3 were not available at the time of this analysis, so that a similar analysis was performed with TRMM VIRS data (Ignatov and Stowe 2000). This analysis has shown that a similar negative bias in this channel is also present, with an average magnitude of $\Delta\tau_3 = -0.01$.

The conclusion from this part of analysis is that the range of sun and view angles beyond $\theta_s, \theta_v = 60^\circ$ may be subject to systematic errors due to unidentified numerical biases (structure of the LUT or interpolation procedure), and should be used with caution. More rigorous ways to resolve these numerical problems should be explored, searching for an optimum choice of the LUT structure, and methods of interpolation. This task is beyond the scope of this study.

8. Concluding remarks

The second-generation aerosol retrieval algorithm was described in detail, with emphasis on its radiative transfer related elements. The Second Simulation of the Satellite Signal in the Solar Spectrum (6S) radiative

transfer model (Vermote et al. 1997a,b) was shown to be more advantageous and better suited for aerosol remote sensing from AVHRR, providing a much wider range of radiative transfer modeling tools and capabilities compared to what had been used formerly (Dave 1973).

The 6S code has been used to analyze the impact of the AVHRR channel's wide spectral response on retrieval accuracy. In particular, analysis of the effective wavelengths suggests that aerosol optical depth retrievals (τ_1 , τ_2 , τ_3) are best reported at the standard set of monochromatic wavelengths of 0.63, 0.83, and 1.61 μm , which most closely represents the channels of a "generic" AVHRR onboard the different NOAA polar orbiting satellites. The respective errors in aerosol optical depths (τ_1 , τ_2 , τ_3) defined this way typically do not exceed $\sim 2\%$. The Ångström exponent derived from (τ_1 , τ_2), may be in error by up to $\delta\alpha \sim \pm 0.25$. For the Ångström exponent derived from (τ_1 , τ_3), this component of error is substantially smaller: $\delta\alpha \sim \pm 0.04$. These estimates are a worst-case scenario for the present algorithm, which first derives two values of aerosol optical depths, and then combines them together to estimate α . For the algorithms based on simultaneous solution, this component of error decreases but never disappears, due to the ever-persistent uncertainties in the inferred aerosol model. Extrapolation to wavelengths beyond the spectral intervals covered by AVHRR is not recommended, as it can introduce additional errors associated with the uncertainty of the inferred or assumed aerosol model.

A new reevaluation of the diffuse oceanic reflectance, ρ^s , based on 6S was done. This analysis suggests that ρ^s in AVHRR channels 1 and 2 are $\rho_1^s = 1.4 \times 10^{-3}$ and $\rho_2^s = 0.15 \times 10^{-3}$. These numbers are lower by 30% and 70%, respectively, than $\rho_1^s = 2.0 \times 10^{-3}$ and $\rho_2^s = 0.5 \times 10^{-3}$, derived by Ignatov et al. (1995) and presently used in the second-generation algorithm. Numerical estimates show that the effect of the differences, $\Delta\rho_1^s = -0.5 \times 10^{-3}$ and $\Delta\rho_2^s = -0.35 \times 10^{-3}$ on the derived τ is within $\sim +(0.2-0.8) \times 10^{-2}$ for τ_1 (about 2%–5% lower than typical τ_1), and $\sim +(0.1-0.5) \times 10^{-2}$ for τ_2 (about 1%–4% lower than typical τ_2). In channel 3a, the diffuse component may be neglected.

Special tests of the numerical performance of the retrieval algorithm have shown that the τ retrievals at high solar zenith and at slant view geometries (beyond 60°) are biased progressively low and should be used with caution. It is not clear at this time what in the retrieval algorithm is causing this error.

The 6S model was evaluated by constructing radiative transfer lookup tables, comparing those to the Dave-based LUTs, and applying them to four large datasets of actual AVHRR measurements. The statistics of differences suggest that the transition from the Dave RT code to the 6S is relatively smooth and with acceptably small systematic and random differences. As a result of this transition, a much more complete, accurate, and

versatile RT modeling tool has replaced the previously used Dave code.

Acknowledgments. The 6S code, and users guide to it, were obtained via anonymous ftp at kratos.gsfc.nasa.gov. Thanks go to Drs. Eric Vermote, Alex Vasilkov, Tom Zhao, and Mr. Ramdas Singh for help with implementation of the 6S and Dave codes; to Mr. John Sapper, who greatly contributed to the development of the mainframe software that was used to download the AEROBS data, used in this study; and to Drs. Nagaraja Rao (deceased), Norm O'Neill, Robert Frouin, Eric Shettle, Andy Heidinger, Robert Arduini, and anonymous reviewers of this paper for helpful advice and discussions. We appreciate the encouragement from Dr. Lee Dantzler, manager of the NOAA/NESDIS Ocean Remote Sensing Program, and from Drs. Bruce Wielicki and Bruce Barkstrom, managers of the NASA/EOS CERES Program (NASA Contract L-90987C), who supported this study.

REFERENCES

- Ångström, A., 1961: Techniques of determining the turbidity of the atmosphere. *Tellus*, **XIII**, 214–223.
- , 1964: The parameters of atmospheric turbidity. *Tellus*, **XVI**, 64–75.
- Bevington, P. R., and D. K. Robinson, 1992: *Data Reduction and Error Analysis for the Physical Sciences*. 2d ed. WCB McGraw-Hill, 328 pp.
- Breon, F. M., 1993: An analytical model for the cloud-free atmosphere/ocean system reflectance. *Remote Sens. Environ.*, **43**, 179–192.
- , and P. Y. Deschamps, 1993: Optical and physical parameter retrieval from POLDER measurements over the ocean using an analytical model. *Remote Sens. Environ.*, **43**, 193–207.
- Cox, C., and W. Munk, 1954a: Statistics of sea surface derived from sun glitter. *J. Mar. Res.*, **13**, 198–227.
- , and —, 1954b: Measurement of the roughness of the sea surface from photographs of the sun's glitter. *J. Opt. Soc. Amer.*, **44**, 838–850.
- , and —, 1955: Some problems in optical oceanography. *J. Mar. Res.*, **14**, 63–78.
- , and —, 1956: Slopes of the sea surface deduced from photographs of sun glitter. *Bull. Scripps Inst. Oceanogr.*, Vol. 6, No. 9, University of California Press, 401–488.
- d'Almeida, G. A., P. Koepke, and E. P. Shettle, 1991: *Atmospheric Aerosols: Global Climatology and Radiative Characteristics*. A. Deepak, 561 pp.
- Dave, J. V., 1973: Development of the programs for computing characteristics of ultraviolet radiation: Scalar case. Tech. Rep. NAS5-21680, NASA GSFC, Greenbelt, MD, 130 pp.
- , 1978: Effect of aerosols on the estimation of total ozone in an atmospheric column from the measurements of its ultraviolet radiance. *J. Atmos. Sci.*, **35**, 899–911.
- Durkee, P. A., F. Pfeil, E. Frost, and E. Shima, 1991: Global analysis of aerosol particles characteristics. *Atmos. Environ.*, **25A**, 2457–2471.
- , and Coauthors, 2000: Regional aerosol optical depth characteristics from satellite observations: ACE-1, TARFOX and ACE-2 results. *Tellus*, **52B**, 484–497.
- Frouin, R., M. Schwindling, and P.-Y. Deschamps, 1996: Spectral reflectance of sea foam in the visible and near-infrared: In situ measurements and remote sensing applications. *J. Geophys. Res.*, **101**, 14 361–14 371.

- Gordon, H., and P. Morel, 1983: *Remote Assessment of Ocean Color for Interpretation of Satellite Visible Imagery: A Review*. Springer-Verlag, 114 pp.
- Guzzi, R., R. Rizzi, and G. Zibordi, 1987: Atmospheric correction of data measured by a flying platform over the sea: Elements of a model and its experimental validation. *Appl. Opt.*, **26**, 3043–3051.
- Higurashi, A., and T. Nakajima, 1999: Development of a two-channel aerosol retrieval algorithm on a global scale using NOAA AVHRR. *J. Atmos. Sci.*, **56**, 924–941.
- , —, B. N. Holben, A. Smirnov, R. Frouin, and B. Chatenet, 2000: A study of global aerosol optical climatology with two-channel AVHRR remote sensing. *J. Climate*, **13**, 2011–2027.
- Husar, R., J. Prospero, and L. Stowe, 1997: Characterization of tropospheric aerosols over oceans with NOAA/AVHRR aerosol optical thickness operational product. *J. Geophys. Res.*, **102**, 16 889–16 909.
- Ignatov, A., 2002: Sensitivity study and information content of aerosol retrievals from AVHRR: Radiometric factors. *Appl. Opt.*, in press.
- , and L. Stowe, 2000: Physical basis, premises, and self-consistency checks of aerosol retrievals from TRMM VIRS. *J. Appl. Meteor.*, **39**, 2259–2277.
- , and —, 2002: Aerosol retrievals from individual AVHRR channels. Part II: Quality control, probability distribution functions, information content, and consistency checks of retrievals. *J. Atmos. Sci.*, **59**, 335–362.
- , —, S. Sakerin, and G. Korotaev, 1995: Validation of the NOAA/NESDIS satellite aerosol product over the North Atlantic in 1989. *J. Geophys. Res.*, **100**, 5123–5132.
- , —, and R. Singh, 1998: Sensitivity study of the Angstrom exponent derived from AVHRR over the oceans. *Adv. Space Res.*, **21**, 439–442.
- Kaufman, Y., 1993: Aerosol optical thickness and atmospheric path radiance. *J. Geophys. Res.*, **98**, 2677–2692.
- Khattak, S., R. A. Vaughan, and A. P. Cracknell, 1991: Sun glint and its observation in AVHRR data. *Remote Sens. Environ.*, **37**, 101–116.
- Kidwell, K., 1995: NOAA polar orbiter data user's guide. [Available from NOAA/NESDIS, Washington, DC 20233.]
- Koepke, P., 1984: Effective reflectance of oceanic whitecaps. *Appl. Opt.*, **23**, 1816–1824.
- Lacis, A. A., and M. I. Mishchenko, 1995: Climate forcing, climate sensitivity, and climate response: A radiative modeling perspective on atmospheric aerosols. *Aerosol Forcing of Climate*, R. T. Charlson and J. Heintzenberg, Eds., John Wiley and Sons, 11–42.
- , J. Chowdhary, M. I. Mishchenko, and B. Cairns, 1998: Modeling errors in diffuse-sky radiation: Vector vs. scalar treatment. *Geophys. Res. Lett.*, **25**, 135–138.
- McClain, C., M. Cleave, G. Feldman, W. Gregg, S. Hooker, and N. Kuring, 1998: Science quality SeaWiFS data for global biosphere research. *Sea Technol.*, **9**, 1–5.
- McClain, E. P., 1989: Global SST and cloud clearing for aerosol optical depth estimates. *Int. J. Remote Sens.*, **10**, 763–769.
- McClatchey, R., R. Fenn, J. Selby, F. Volz, and J. Garing, 1971: Optical properties of the atmosphere (revised). AFCRL-71-0279, Environmental Research Paper 354, USAF, 91 pp.
- Mishchenko, M. I., I. V. Geogdzhayev, B. Cairns, W. B. Rossow, and A. Lacis, 1999: Aerosol retrievals over the oceans by use of channels 1 and 2 AVHRR data: Sensitivity analysis and preliminary results. *Appl. Opt.*, **38**, 7325–7341.
- Monahan, E. C., and I. Ø. Muirchearthaigh, 1980: Optimal power-law description of oceanic whitecap coverage dependence on wind speed. *J. Phys. Oceanogr.*, **10**, 2094–2099.
- Moore, K., K. Voss, and H. Gordon, 2000: Spectral reflectance of whitecaps: Their contribution to water-leaving radiance. *J. Geophys. Res.*, **105** (C3), 6493–6499.
- Morel, A., 1988: Optical modeling of the upper ocean in relation to its biogenous matter content (Case I waters). *J. Geophys. Res.*, **93** (C9), 10 749–10 768.
- , and L. Prieur, 1977: Analysis of variations in the ocean color. *Limnol. Oceanogr.*, **22**, 709–722.
- Neckel, H., and D. Labs, 1984: The solar radiation between 3300 and 12500 Å. *Sol. Phys.*, **90**, 205–258.
- O'Brien, D. M., and R. M. Mitchell, 1988: Retrieval of surface wind speed and aerosol optical depth over the oceans from AVHRR images of sun glint. *J. Appl. Meteor.*, **27**, 1395–1403.
- Quenzel, H., and M. Kaestner, 1980: Optical properties of the atmosphere: Calculated variability and application to satellite remote sensing of phytoplankton. *Appl. Opt.*, **19**, 1338–1344.
- Rao, C. R. N., and J. Chen, 1996: Post-launch calibration of the visible and near-infrared channels of the Advanced Very High Resolution Radiometer on the NOAA-14 spacecraft. *Int. J. Remote Sens.*, **17**, 2743–2747.
- , L. Stowe, and P. McClain, 1989: Remote sensing of aerosols over oceans using AVHRR data: Theory, practice and applications. *Int. J. Remote Sens.*, **10**, 743–749.
- Royer, A., N. O'Neill, A. Davis, and L. Huebert, 1988: Comparison of radiative transfer models used to determine atmospheric optical parameters from space. *Proc. SPIE*, **928**, 118–135.
- Shettle, E. P., and R. W. Fenn, 1979: Models for the aerosols of the lower atmosphere and the effects of humidity variations on their optical properties. Environmental Research Paper 675, AFGL-TR-79-0214, 94 pp.
- Siegel, D., M. Wang, S. Maritorena, and W. Robinson, 2000: Atmospheric correction of satellite ocean color imagery: The black pixel assumption. *Appl. Opt.*, **39**, 3582–3591.
- Soufflet, V., D. Tanre, A. Begue, A. Podaire, and P. Y. Deschamps, 1991: Atmospheric effects on NOAA AVHRR data over Sahelian regions. *Int. J. Remote Sens.*, **12**, 1189–1203.
- Stowe, L. L., A. Ignatov, and R. Singh, 1997: Development, validation and potential enhancements to the second generation operational aerosol product at NOAA/NESDIS. *J. Geophys. Res.*, **102**, 16 923–16 934.
- , H. Jacobowitz, G. Ohring, K. Knapp, and N. Nalli, 2002: The Advanced Very High Resolution Radiometer Pathfinder Atmosphere (PATMOS) climate dataset: Initial analyses and evaluation. *J. Climate*, in press.
- Tanre, D., B. N. Holben, and Y. J. Kaufman, 1992: Atmospheric correction algorithm for NOAA-AVHRR products: Theory and applications. *IEEE Trans. Geosci. Remote Sens.*, **30**, 231–248.
- , Y. J. Kaufman, M. Herman, and S. Matoo, 1997: Remote sensing of aerosol properties over oceans using the MODIS/EOS spectral radiances. *J. Geophys. Res.*, **102**, 16 971–16 988.
- Teillet, P. M., 1990: Rayleigh optical depth comparisons from various sources. *Appl. Opt.*, **29**, 1897–1900.
- Vermote, E., D. Tanre, J. L. Deuze, M. Herman, and J. J. Morcrette, 1997a: Second Simulation of the Satellite Signal in the Solar Spectrum, '6S': An overview. *IEEE Trans. Geosci. Remote Sens.*, **35**, 675–686.
- , —, —, —, and —, 1997b: Second Simulation of the Satellite Signal in the Solar Spectrum (6S). 6S user's guide, version 2, 218 pp. [Available via anonymous FTP at kratmos.gsfc.nasa.gov.]
- Viollier, M., D. Tanre, and P. Y. Deschamps, 1980: An algorithm for remote sensing of water color from space. *Bound.-Layer Meteor.*, **18**, 247–367.
- Wagner, R., S. Nemesure, and S. E. Schwartz, 1997: Aerosol optical depth over oceans: High space- and time-resolution retrieval and error budget from satellite radiometry. *J. Atmos. Oceanic Technol.*, **14**, 577–590.
- World Climate Programme, 1983: Report of the expert meeting on aerosols and their climatic effects. WCP-55, World Meteorological Organization, Geneva, Switzerland, 83 pp.
- , 1986: A preliminary cloudless standard atmosphere for radiation computations. WCP-112, WMO/TD-N24, World Meteorological Organization, Geneva, Switzerland, 83 pp.